INFRARED 8-13μ SPECTROSCOPY OF THE MOON AND SOME COLD SILICATE POWDERS

Thesis by

Alexander Franklin Hermann Goetz

In Partial Fulfillment of the Requirements

For the Degree of

Doctor of Philosophy

California Institute of Technology

Pasadena, California

1967

(Submitted December 30, 1966)

ACKNOWLEDGMENTS

The writer received assistance from many persons during the course of this research. In particular, he is indebted to Dr. Bruce Murray, the writer's thesis advisor, for originally suggesting the problem and for his able guidance and well-timed optimism which helped immensely in completing this project.

Mr. James Westphal was particularly helpful in the design and fabrication of all the instruments as well as in discussions about the data reduction process. His willing and able support under all circumstances kept the investigation moving in spite of numerous difficulties.

Dr. Leon Silver kindly supplied the samples used in the laboratory investigations and gave expert advice on the preparation and handling of rock powders.

Mr. Curtis Bauman was instrumental in designing and supervising the building of the vacuum chamber as well as advising the writer on vacuum problems.

The writer is indebted to Dr. Gerry Neugebauer for discussions and constructive criticism during the preparation of this manuscript.

The secretarial and editorial assistance of the writer's wife, Nancy Goetz, is gratefully acknowledged.

The writer was supported by a National Aeronautics and Space Administration Traineeship Grant for the duration of this investigation.

ABSTRACT

Laboratory investigations were made of the spectral emission properties of a limited number of silicate powders in vacuum and surface temperatures of 180-240°K. The effect on the emission spectrum of mineral composition, powder grain-size, surface contamination and thermal gradient was studied.

The low sample surface temperature enhanced the spectral contrast of quartz but had little effect on spectra of rock materials. In general, there was a decrease in spectral contrast with decreasing sample grain-size. However, this effect was more pronounced for individual mineral samples than for rock samples. When the particle size was reduced to less than 38μ individual rock types could not be identified. However, quartz bearing or generally acidic rocks could be differentiated from quartz free or generally basic rock types. A quartz sample which had been contaminated by iron oxide did not lose its spectral features in spite of being visibly colored. The effect of a thermal gradient in the sample on its emission spectrum was shown to be negligible.

Differential 8-13μ spectroscopy of 22 lunar points, spanning the major types of lunar features, was undertaken to determine if compositional differences or age are evidenced in the 8-13μ emission spectra of the features. A method was devised to remove precisely the atmospheric absorption and allow the integration of many spectra in order to reduce uncertainties caused by atmospheric absorption fluctuations and detector noise.

Twenty of the 22 points showed no spectral differences greater than 1%. Two points, Plato and Mare Humorum, showed definite, consistent spectral differences from the rest of the points measured, at the short wavelength end of the spectrum.

The interpretation made here of these results is that these two points have significantly fresher surfaces exposed which still show some spectral contrast or they are compositionally different from their surroundings. In the former case the anomalous areas must be partially covered with a non-silicate material in order to be consistent with the data obtained. If the points are compositionally different and the uniform areas show spectral contrast, the uniform areas must contain quartz and the anomalous areas are then more basic in composition than the uniform areas. The alternative to these two possibilities is that some process, perhaps an effect of the solar wind, is operating in such a way as to produce spectra which are unknown and hence can be falsely interpreted.

TABLE OF CONTENTS

I. INTRODUCTION

In the last few years there has been a growing interest in the use of mid-infrared emission data from the moon and planets as a diagnostic tool. Relatively little spectroscopic ground-based astronomy has been undertaken in the 8-13μ wavelength region (Sinton and Strong, 1960; Hunt and Salisbury, 1964; Murcray, 1965) because of the difficulty in the interpretation of data taken through a variable, absorbing and emitting atmosphere. However, such spectroscopy should be pursued further, since laboratory work on silicate materials (Van Tassel and Simon, 1964; Lyon, 1964, Conel, 1965) has demonstrated the potential value of spectroscopic emission studies of planetary surfaces in determining their mineralogic composition.

The primary purpose of this investigation was to determine if any departures from a graybody emission in the 8-13μ wavelength region occur in representative areas on the lunar surface and to what extent these departures can provide information about the distribution of mineralogic phases. In connection with the analysis of lunar spectra, laboratory investigations of the spectral emission of selected silicate powders were undertaken. Experiments were made under conditions of vacuum and at temperatures and temperature gradients simulating more closely those on the lunar surface than in previous investigations.

The first experiments designed to determine the presence of silicates on the moon were made by Pettit and Nicholson (1930). They determined that the emissivity between 8 and 10μ was the same

as between 8 and 14μ and concluded that if silicates were present they must be in a finely divided or porous state. Sinton and Strong (1960) made high resolution (.08μ) 8-13μ spectra of the moon in the course of investigations of the atmosphere of Mars, but did not make any inferences about the lunar surface, which they used as a standard source.

In response to the renewed interest in the determination of the composition of the lunar surface from infrared spectra, Hunt and Salisbury (1964) made mid-infrared spectral scans of selected lunar regions in the 16-24μ region. Although the portion of the lunar surface scanned was relatively large (80 x 480 km) and only a single beam system was used, the authors reported spectral differences between the four areas surveyed, which they attributed to compositional differences. The magnitude of the differences is not given but from a figure shown they appear to be as large as 10%.

Murcray (1964) has made 8-14μ spectra of an area encompassing the entire equatorial region (latitude ± 30°) of the full moon in an attempt to make absolute emissivity determinations. He reports significant departures from unit emissivity. However, his wavelength resolution (.2μ) was not sufficient to resolve the 9.6μ ozone band and minimize its interference.

Most recently, Hunt et al. (1966), using a different technique employing reststrahlen reflection plates of quartz and olivine, have reported differences in the emission properties of Mare Serenitatis and Mare Tranquilitatis amounting to 1 or 2%. Unfortu-

nately, this method is dependent on the temperature of the surface measured. No allowance is made for the variable emission from the sky or the telescope in any of the post-1963 observations.

The present study was designed to overcome some of the uncertainties in the 8-13μ spectroscopy of the moon which are introduced by the variable emission and absorption of the earth's atmosphere. Reduction of the emission component was accomplished by using a dual-beam photometer, and the absorption was compensated for by comparing points on the lunar surface using a differential technique. The spatial resolution as well as the wavelength resolution have been improved over that of previous workers by the use of a liquid hydrogen-cooled, mercury-doped germanium quantum detector.

II. INFRARED PROPERTIES OF SILICATES

All rock-forming silicates have basic lattice vibration frequencies in the 8-13μ wavelength region. The reststrahlen or residual rays are due to the fundamental Si-0 stretching vibrational mode which gives rise to high absorption and hence high reflectivity. This behavior is illustrated by the equation for normal reflection

$$R = \frac{(n-1)^2 + k^2}{(n+1)^2 + k^2}$$

where n is the index of refraction and k the extinction coefficient. Figure 1, taken from Simon and McMahon (1953), shows that the wavelength positions of maximum absorption and maximum reflection do not coincide exactly because of the behavior of n close to the vibrational frequency.

The reststrahlen wavelengths for silicate materials are dependent on the Si/0 ratio or degree of polymerization of the $Si0_4$ tetrahedron. Strong quartz ($Si0_2$) reflection peaks lie at the short wavelength end of the band, at about 8.5 and 8.8μ, while the reflection peaks for olivine $(Fe, Mg)_2\ Si0_4$ are found at 10.2 and 10.6μ. Weaker bands for quartz are located at 12.4μ and for olivine at 12.0μ. Materials with intermediate Si/0 ratios have reflection peaks which lie between those of the above end members. Figure 2 is a reproduction of Figure 13 in a paper by Launer (1952) showing the wavelength ranges of strong infrared absorption bands of silicon-oxygen groups. Absorption spectra are used in the identification of silicate materials (Launer, 1952; Lyon et al., 1959). Hovis and Callahan

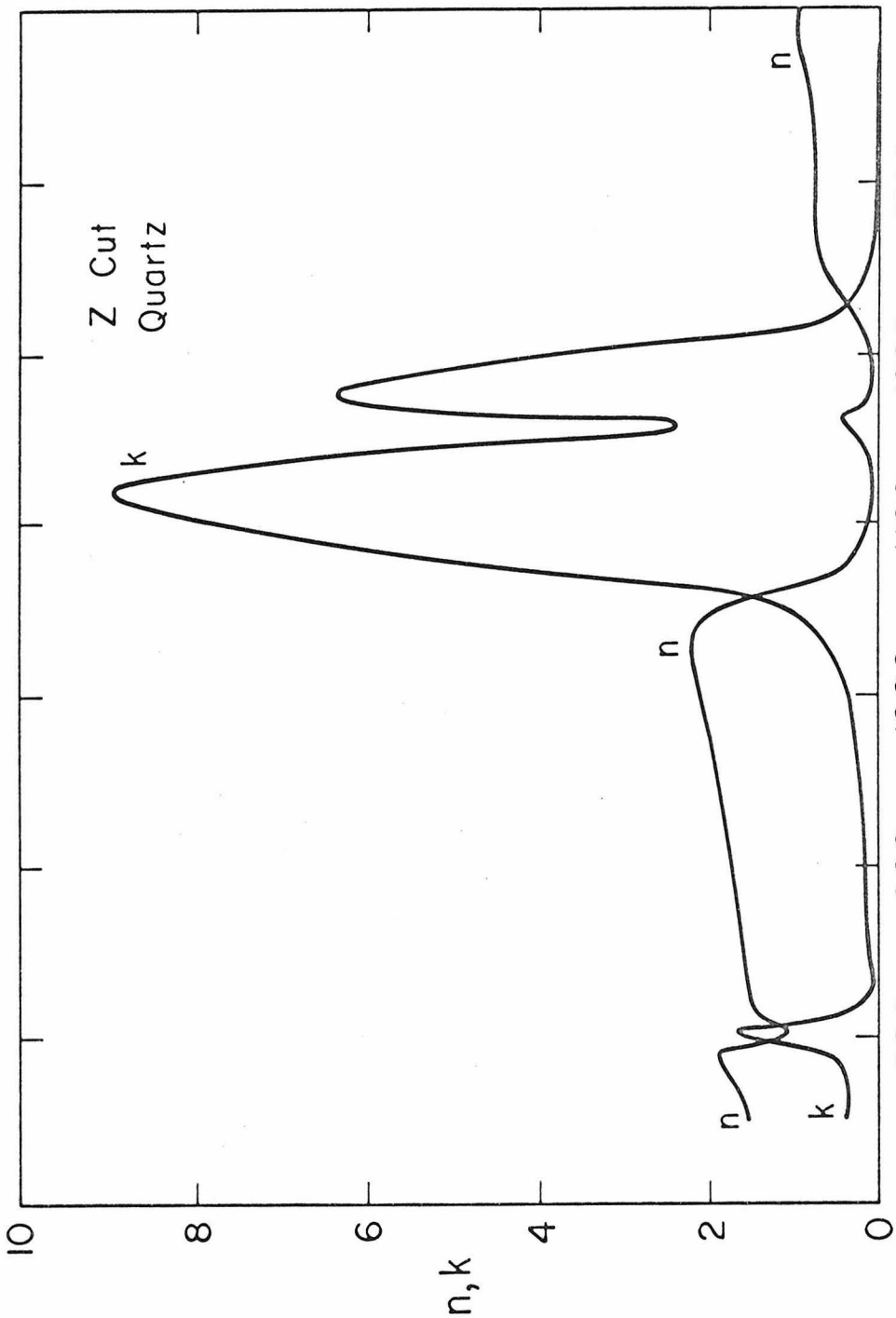

Figure 1. Behavior of the optical constants n and k at the reststrahlen wavelengths for Z-cut quartz (Simon and McMahon). To convert cm^{-1} to microns, divide 10^4 by ν .

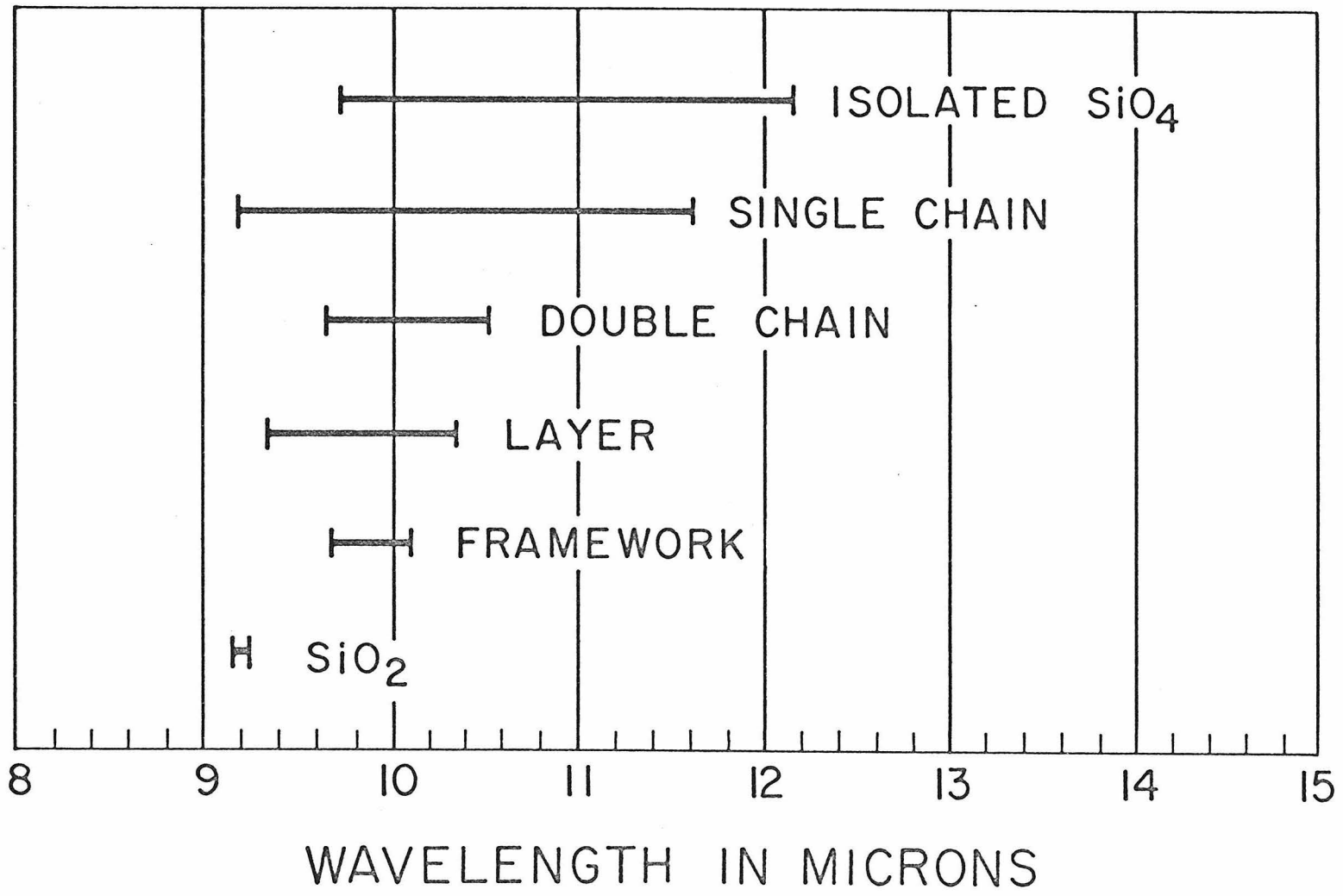

Figure 2. Wavelength ranges of strong infrared absorption bands of silicon-oxygen groups (Launer)

(1966) have shown that the spectrum of a rock or mineral composites can be represented by the average of the spectra of the individual mineral constituents.

According to Kirchhoff's law, under conditions of thermodynamic equilibrium, for opaque materials

$$R(\lambda) + A(\lambda) = 1$$

and

$$\epsilon(\lambda) = A(\lambda) = 1 - R(\lambda)$$

where R is the reflectivity, A is the absorptivity and ϵ is the emissivity. Measurements of the emitting properties of polished silicate surfaces yield information about composition equal to that of reflection measurements (Lyon, 1964). However, this is not true in the case of rough surfaces or powdered specimens. Reflection spectra cannot be used to predict the emissivity behavior of powdered materials.

Recently, emphasis has been placed on the measurement of the spectral emission of silicate dusts and powders with application to remote determination of soil composition on the earth, as well as on the moon and planets (Lyon, 1964; Van Tassel and Simon, 1964; Conel, 1965; Lyon, 1965). The single most important characteristic of the emission from rough or powdered surfaces is their reduced spectral contrast. The spectral contrast decreases with decreasing grain size. The emission from dusts with grain sizes less than about 50 microns is close to that of a graybody* exhibiting

---

*A graybody is defined as an object having an emissivity independent of wavelength and less than unity.

practically no spectral features. Generally the positions of emission minima remain constant in the transition from polished to roughened surfaces, although the spectral features are usually broadened. However, Conel (1965) reports that in rocks containing quartz, emission minima appear to shift with decreasing grain size because of the reststrahlen contribution of quartz, which remains strong even for small grain sizes. While it may not be possible to differentiate between individual rock types in the dust form, it is possible to separate a quartz-containing or generally acidic-type rock from a quartz-free or generally basic rock.

III. LABORATORY STUDIES

Extensive studies of the mid-infrared spectral behavior of silicate materials have been carried out by several investigators (Van Tassel and Simon, 1964; Conel, 1965; Lyon, 1965), in particular by Lyon (1964). These measurements were made at atmospheric pressure and at temperatures near or greater than lunar sub-solar point temperatures of 370-400°K to reduce interference from room temperature sources.

For the laboratory measurements a special apparatus was constructed in order to more closely simulate lunar surface conditions of temperature, pressure, and thermal gradient. The apparatus is described in detail in Appendix I.

Briefly, the sample is placed inside a vacuum chamber and is heated from below. Its surface radiates into a cavity maintained at liquid nitrogen temperature (77°K). The gradient created is positive going into the sample, and surface temperatures, for 2mm thick samples, range from 180 to 240°K, depending upon the bath temperature and the thickness and thermal conductivity of the sample. This surface temperature lies within the range of lunar temperatures found near the terminator and also those measured during an eclipse (Pettit, 1940; Saari and Shorthill, 1963, 1966). The gradient is not inconsistent with proposed eclipse cooling models (Ingrao et al., 1965).

The spectral emittance of a sample, $\epsilon(\lambda)$, is defined as the ratio between the radiance of the sample and the radiance of a black-

body at the same temperature at a given wavelength

$$\epsilon(\lambda) = \frac{B_s(\lambda)}{B_{bb}(\lambda)} \quad .$$

To determine the emittance of the sample, the surface temperature must be measured.

The thermal conductivity of silicate powders is very low, approximately 10^{-5} to 10^{-6} cgs (Watson, 1964). It is therefore, not possible to measure accurately the surface temperature by means of thermocouples or similar devices because of the high point contact thermal resistance.

In silicate powders the departures from graybody emission are relatively sharp (0.2-2μ wide) with respect to shifts in the Planck function curve due to changes in temperature. In the 8-13μ region these powders exhibit emittances approaching unity at several wavelength intervals. Using a blackbody reference at a known temperature to determine system response, it is possible to fit the sample spectrum, in the high emittance wavelength intervals, to a Planck function curve with a digital computer. The wavelength interval used in these measurements was 7.8-8μ. With the knowledge of the sample surface temperature the "relative" spectral emittance can be calculated. The term relative is used, since the actual kinetic surface temperature is not known and the assumption of unit emittance at given wavelengths may not always be valid. It is not necessary to know the absolute emittance values for compositional analysis. The

computer data yield the relative departures from graybody emission, and it is these that are important in identifying composition. Figure 3a, b demonstrates the method used for determining relative emittance.

The following points were emphasized in the laboratory program:

1. Effect of mineralogy on emission spectra.
2. Effect of grain-size on spectral contrast.
3. Effect of surface contamination on spectral contrast.
4. Effect of a low surface temperature and a thermal gradient in the sample on its emission spectrum.

These particular questions were chosen because of their relevance to the interpretation of the results of the lunar measurements. A comprehensive study of the first two questions, with data in suitable form for use in the reduction of the lunar data, has not been published in the literature. In order to obtain this information, it was necessary in some cases to duplicate previous work.

3.1 Mineralogy Effects

The first two questions have been investigated in detail by previous workers (Van Tassel and Simon, 1964; Lyon, 1964; Conel, 1965). For this reason only a small number of rock and mineral types were chosen for study (cf. Appendix II). This number was sufficient to test adequately the ability of the instruments used in the telescopic study to detect reststrahlen features and small differences in emissivity.

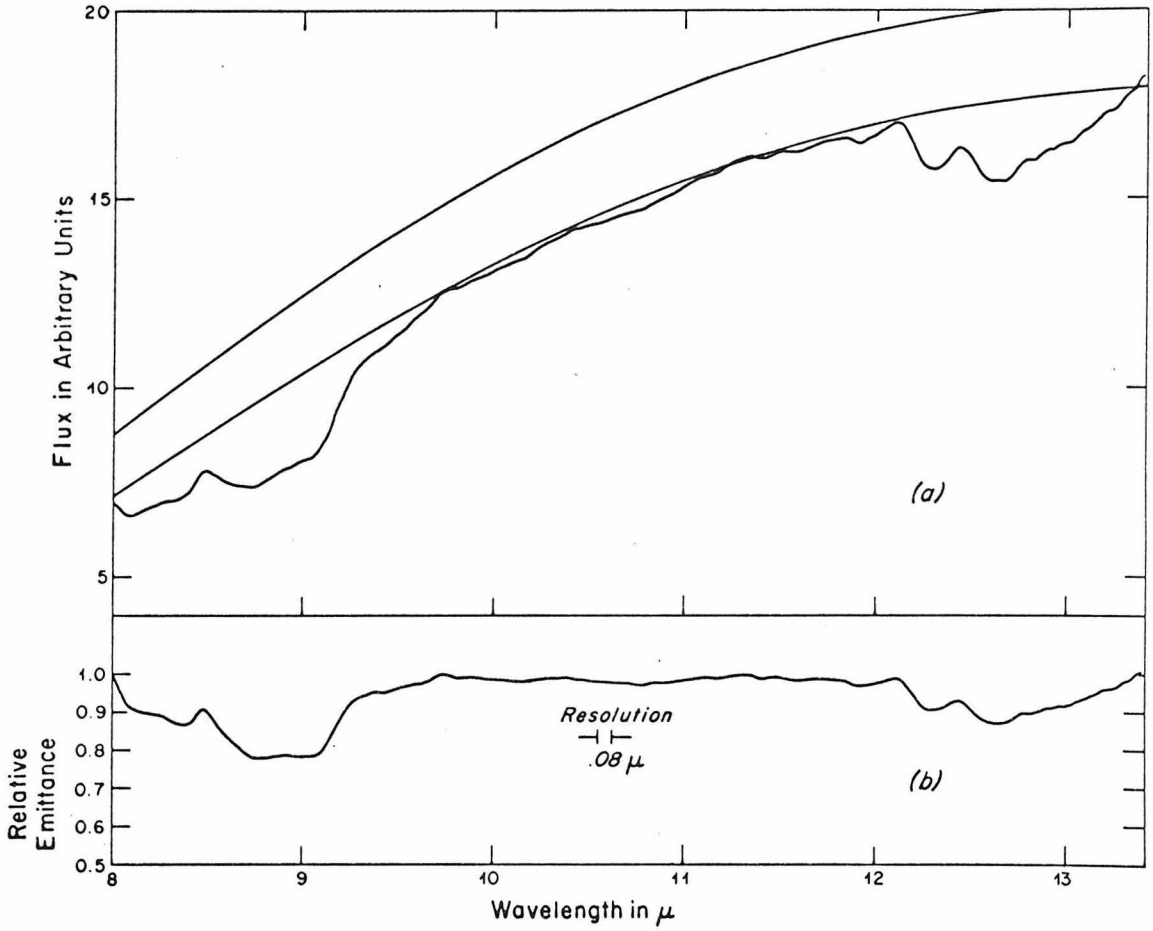

Figure 3a. Emission spectrum of quartz powder with closest fitting blackbody curve. Upper curve is a blackbody curve .5°K higher in temperature.

Figure 3b. Relative emittance of the quartz sample calculated as the ratio of the sample curve and closest fitting blackbody curve.

Figure 4a shows the effect of mineralogy on the position of the reststrahlen wavelengths for quartz and olivine. These minerals represent the end members as far as the degree of polymerization of the SiO_4 tetrahedron is concerned. Figure 4b shows the emission curves for an acidic rock (gneiss with quartz monzonite composition) and a basic rock (basalt). As indicated in the previous section, the emission curves of rock samples have a relatively smooth appearance because of the averaging of the emission curves of the individual mineral constituents. In the case of the quartz monzonite the characteristic quartz lines between 8.4 and 9.2μ are visible. The basalt sample does not exhibit any strong lines, but rather a general decrease in emission between 10.5 and 11.5μ. Figure 5 shows spectra of an acidic rock, San Marcos Gabbro. In spite of the coarse particle size (.3-.5 mm) the spectral contrast is not high. This is to be expected, since one is working with mineral assemblages in rocks rather than individual minerals. However, the shift in the emission minimum to longer wavelengths, in transition from the acidic to the basic rock type, is readily apparent.

3.2 Grain-size Effects

The effect of grain-size on the spectral contrast is more pronounced for individual minerals than for rock materials. Figure 6 shows the effect of grain-size on the spectral contrast for quartz. The contrast remains reasonably constant until the smallest grain-size range, less than 37 microns, is reached. At this point, the spectral contrast is greatly diminished but not obliterated. Van Tassel

Figure 4a. Relative emittance curves for quartz (SiO_2) and olivine $(Mg, Fe)_2SiO_4$ showing the effect of the silicon-oxygen ratio on the position of emission minima.

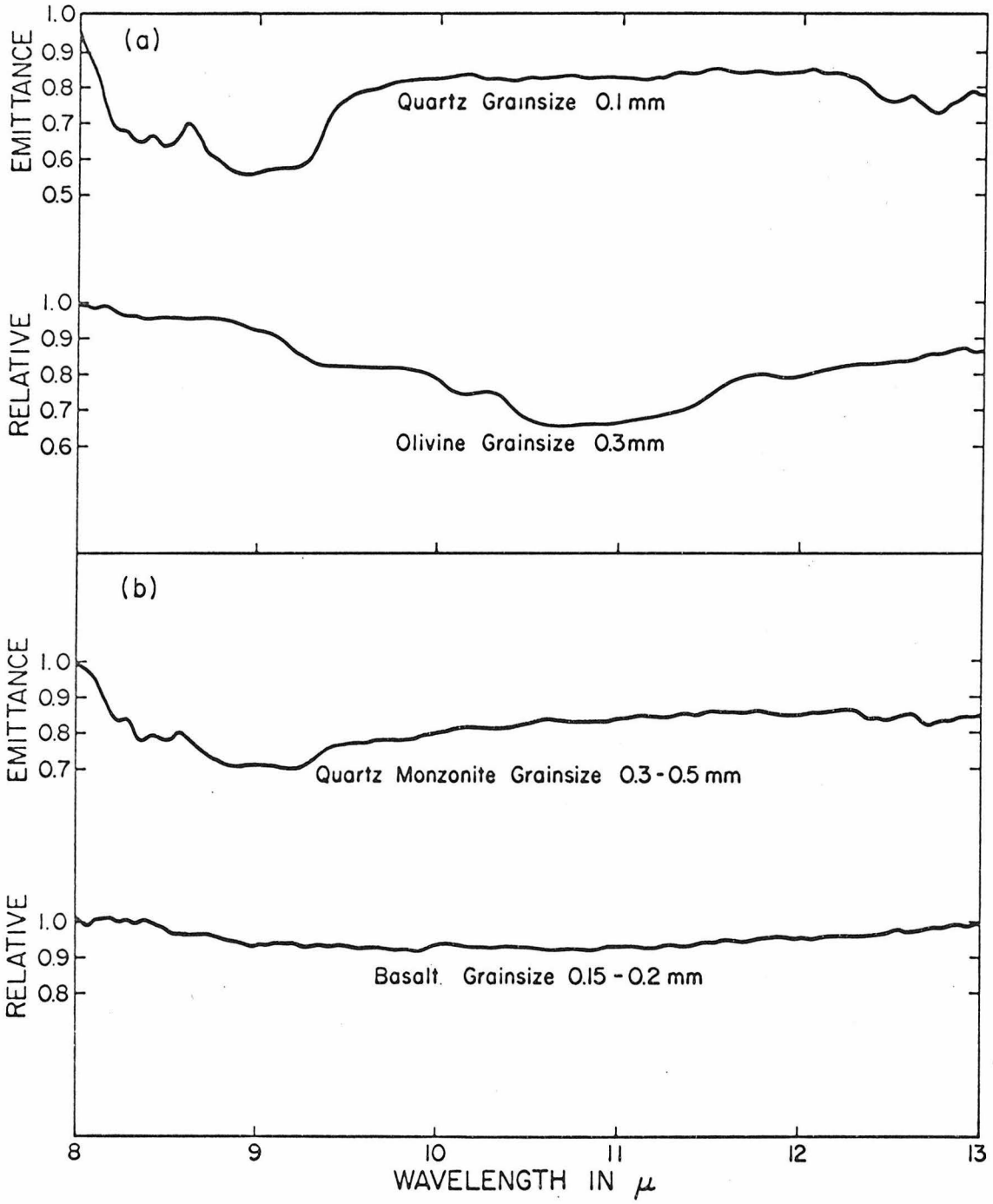

Figure 4b. Relative emittance curves for an acidic rock, quartz monzonite, and a basic rock, basalt.

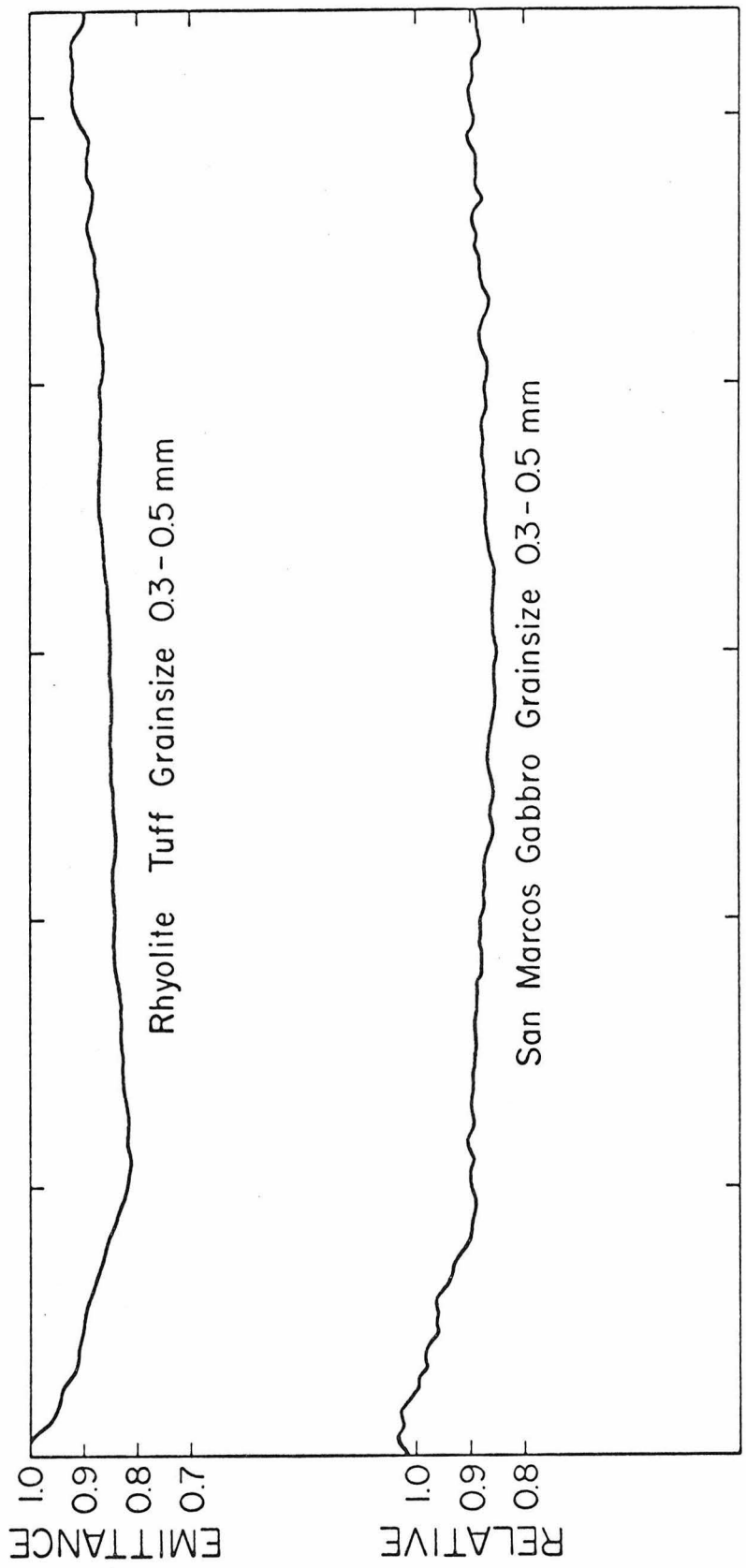

Figure 5. Relative emittance curves for an acidic rock, rhyolite tuff containing 90% SiO_2 glass, and a basic rock, San Marcos Gabbro.

Figure 6. Effect of grain-size on the spectral contrast of quartz shown on the left and two acidic rocks shown on the right.

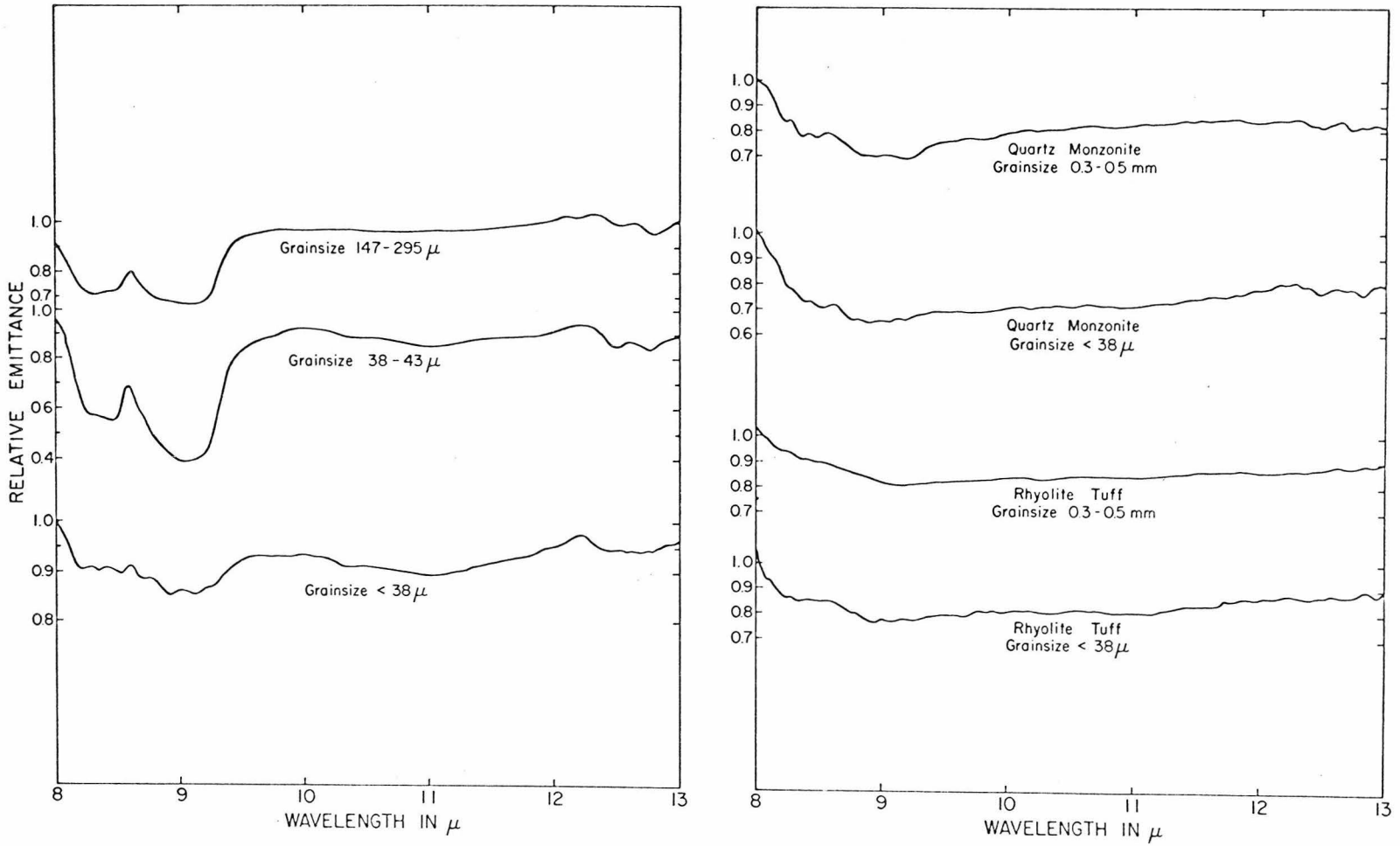

and Simon (1964) have suggested that the gradual diminishing of spectral contrast with the decrease in grain-size is due to scattering effects which become most effective as the grain-size approaches the wavelength of the emitted radiation. They reported essentially perfect graybody emission for samples with particle sizes centering around one to two microns.

Figure 6 also shows the effect of grain-size on the emission spectrum of two rock specimens, rhyolite tuff and quartz monzonite. In the case of the rhyolite, little if any real differences can be seen. The spectrum of the sample having a grain-size less than 37 microns has a poorer signal-to-noise ratio, because its surface temperature was only 204°K, 33°K less than that of the coarse-grained sample. The emission minimum near 9μ is present in both spectra. In the case of the quartz monzonite spectra the emission minima due to quartz are better defined in the coarse than in the fine sample. This figure again illustrates the previously mentioned predominance of the quartz contribution to the overall emission spectrum of a quartz-bearing rock sample.

3.3 Surface Contamination Effects

The question of the effect of surface contamination has important bearing on the analysis of lunar infrared spectra. Wehner et al. (1963a, b) have proposed that the sputtering action of the solar wind preferentially removes the lighter elements, such as oxygen, from oxide powders. This sputtering action increases the concentration of metals on the material surface and causes darkening in the visible wavelengths. Hapke (1966) has proposed a lunar surface model

in which silicate materials are darkened by the sputtering action by the deposition of a non-stochiometric silicate compound deficient in oxygen on the underside of the surface grains. No studies of the infrared properties of laboratory irradiated powder materials have been published.

No irradiated sample material was available for analysis. However, two types of contaminated samples were studied to determine whether a surface coating of foreign material would affect the emission spectrum of the sample.

One sample was a quartz powder, having a grain-size less than 37 microns. To the eye the sample had a gray-brown appearance which resulted from oxidation of the iron crusher contaminants. The sample had a similar appearance under the binocular microscope, and it was obvious that the coloration was not due to individual iron oxide particles in the same size range as the quartz sample. The coloration appeared to be due to a fine coating on the individual quartz grains. An emission spectrum was made of this material. A portion of the contaminated material was leached in 2N HCl at 50^{o}C for three hours. After washing, the quartz powder recovered its normal brilliant white appearance. The spectra of both samples are shown in Figure 7. No appreciable difference in spectral contrast is noted. The iron oxide which produced the coloring at visible wavelengths had no effect on the infrared emission characteristics.

Figure 7 also shows the effects of weathering on a quartz monzonite. The upper curve is the emission spectrum of a coarsely ground quartz monzonite gneiss. The lower spectrum came from

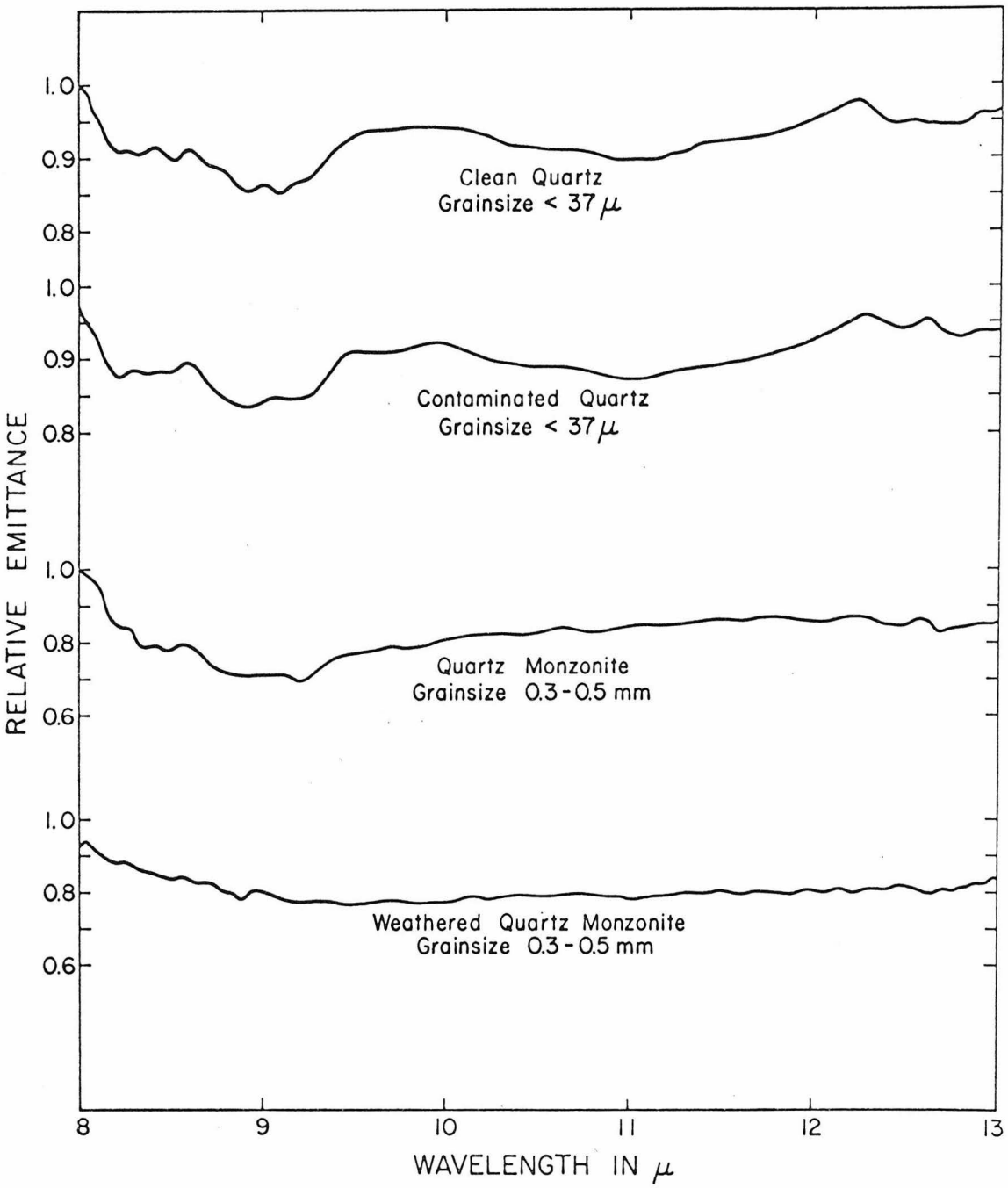

Figure 7. Effect of minor contamination of quartz by iron oxide and the effect of weathering on the spectral contrast of quartz monzonite.

strongly weathered material of the same composition and collected in an adjacent locality. The spectrum of the weathered material has little spectral contrast and the quartz reststrahlen peaks are not visible. The weathered sample had a red-brown coloration and was in granulated form when collected. The sieving process, which retained sizes greater than .3 mm and less than .5 mm, could be expected to cause mineral fractionation and preferential loss of quartz. However, a subsequent count showed that the sample still contained 20% quartz. The spectrum retained the characteristics of emission from an acidic rock type, in spite of the partial alteration of the feldspars and micas to various clay minerals. The loss of contrast can be attributed to the coating of the quartz grains with a layer of very finely divided clay material in aggregate form.

3.4 Temperature and Thermal Gradient Effects

The effect of temperature on the position of the reststrahlen wavelengths was expected to be very small (Su et al., 1962). Measurements showed that the 1088 cm^{-1} absorption band of quartz was only shifted 2 cm^{-1} over a sample temperature range of 4.2 to 523°K. However, an increase in spectral contrast is expected because of the decreasing width and deepening of the resonance lines with decreasing temperature (Simon and McMahon, 1953).

The interest in the effects of a high thermal gradient on the emission properties of silicate powder surfaces was based on two facts:

1. During the umbral phase of a lunar eclipse a strong thermal gradient, positive with depth, is present on the lunar surface.
2. It is very difficult, if not impossible, to measure the radiation from a low thermal conductivity powder under isothermal conditions.

In order to make a rough theoretical calculation of the effect of a temperature gradient on the emission of a powder sample, the sample was modeled by a series of plane parallel slabs, each having a different temperature T. The expressions for the emissivity and transmissivity of partially transmitting bodies were taken from McMahon (1950). In this case Kirchhoff's law was expanded to yield the expressions

$$\epsilon(\lambda) = \frac{[1 - R(\lambda)]\ [1 - D(\lambda)]}{1 - R(\lambda)\ D(\lambda)} \qquad (1)$$

$$D^{*}(\lambda) = D(\lambda)\ \frac{[1 - R(\lambda)]^2}{1 - R^2(\lambda)\ D^2(\lambda)} \qquad (2)$$

where R is the reflectivity, D the transmissivity measured from the optical constants and D^{*} the apparent transmissivity. The radiant flux density emitted by the surface for this model can be written as

$$W(\lambda)\Delta\lambda = \Delta\lambda\ \epsilon(\lambda) \sum_{k} B(\lambda, T_k) D^{*k}(\lambda)$$

where B is the Planck function evaluated at temperature T_k of the k^{th} slab. For purposes of calculation, 40 micron thick slabs and a

temperature increase of $3^{o}K$ per slab were assumed for the model. These values were taken from laboratory measurements on a 1.3 mm thick quartz sample containing particles in the size range 38 to 43 microns.

Simon and McMahon (1953) give values for the optical constants n and k and R for quartz. However, for small values of k near 11μ it is not possible to take accurate values from their plotted curves. A comparison of the optical constants for crystalline quartz and quartz glass in the same paper showed a close correlation in the values of n and k. A recent paper by Cleek (1966) gives values for the absorption coefficient for a number of silicate glasses. Figure 8 is a reproduction of Cleek's values for quartz glass.

The transmissivity is given by

$$T(\lambda) = e^{-\alpha(\lambda)d}$$

where d is the slab thickness. The smallest value of α in Figure 8 is 67 mm^{-1} at 11μ. At this wavelength, for d = .04 mm one obtains

$$T(11\mu) = .067 \quad .$$

Evaluating equations (1) and (2) shows that W(11μ) is less than 1% greater than the radiant flux density calculated for an opaque sample having the same surface temperature. At wavelengths where α is greater, the difference is proportionately smaller. The assumption of plane parallel slabs, normal incidence, and thermodynamic equilibrium yields the ideal case which would result in the highest value for the enhancement by a positive gradient. In the case of a

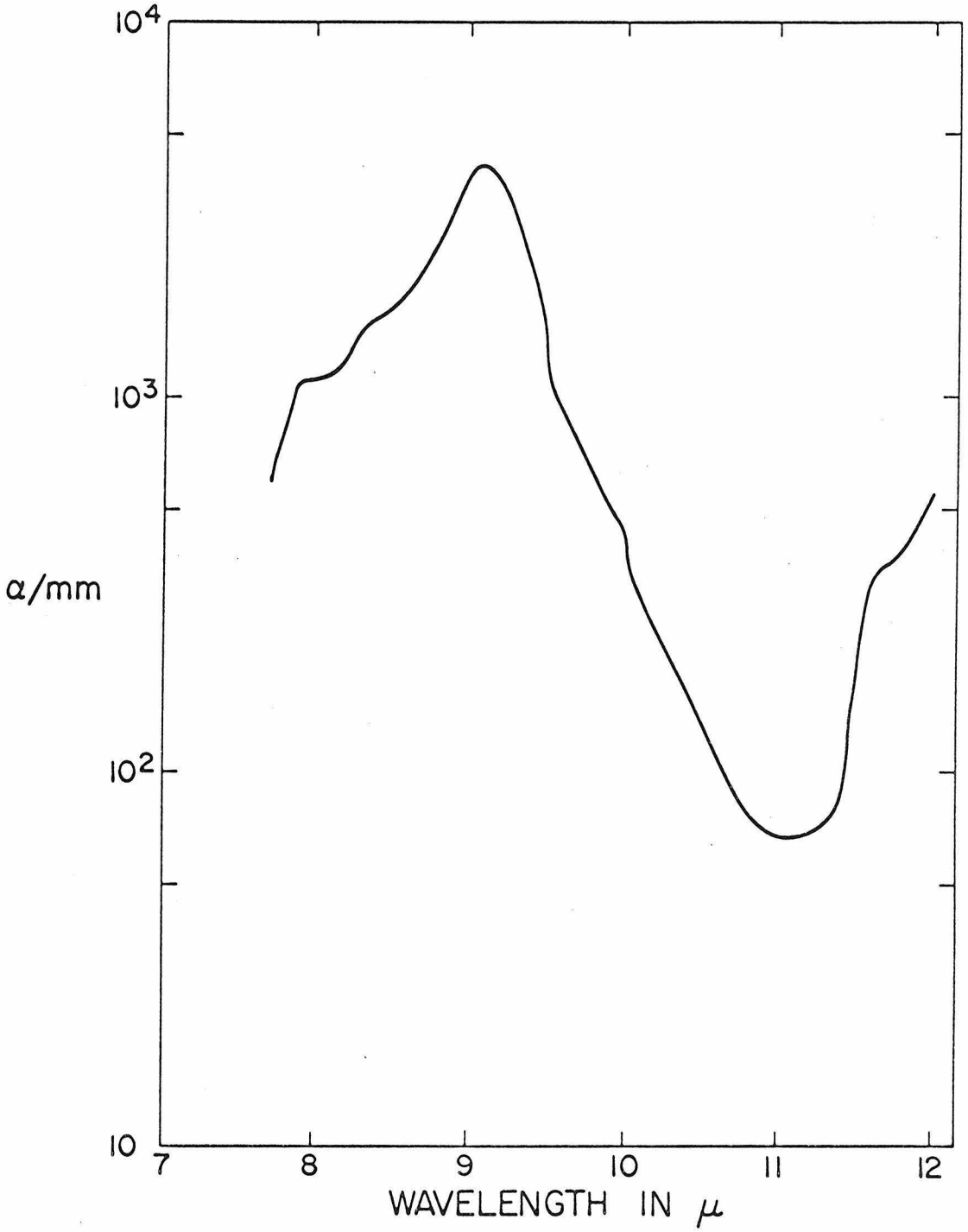

Figure 8. Wavelength dependence of the absorption coefficient for SiO_2 glass (Cleek).

natural powder sample, scattering by the rough grain surfaces further reduces the contribution from the warmer grains underneath the surface. The influence of a temperature gradient on the emission spectrum of these particles is therefore negligibly small.

3.5 Conclusions

Emission spectra of silicate materials taken under conditions of vacuum and low temperature (200°K) do not differ appreciably from those taken by other workers under conditions of high temperature (400-700°K) and atmospheric pressure. The spectra of quartz powder taken at low temperatures exhibit higher spectral contrast than those taken by previous workers. However, this effect does not appear to extend to spectra of rock powders.

While the spectral information obtainable from silicate powders decreases rapidly with decreasing grain-size, even in powder form (grain-size $< 37\mu$), acidic rock types can be distinguished from basic rock types, particularly if the former contain quartz.

Contamination, although studied only superficially, does not appear to be important if the contaminating layer is optically thin in this wavelength region.

3.6 Error Analysis

The main sources of error in the laboratory measurements were: (1) Emission from sources other than the sample; (2) surface temperature measurement; (3) emissivity of the calibration unit; (4) linearity of the detection system; (5) wavelength reproducibility and calibration; and (6) detector noise.

The two possible sources of stray emission were the calibration unit and the energy emitted by the spectrometer at room temperature being reflected off the sample and entering the spectrometer as a chopped signal. Although the calibration unit was removed from the beam, some radiative heating of the sample was detected from this source which had been held at 273°K. Therefore, in all the measurements discussed above, the calibration unit was cooled by liquid nitrogen when sample spectra were being taken. The room temperature energy arriving in the well-baffled, f16 beam is scattered by the surface. If Lambert scattering is assumed, then the energy scattered back into the f16 beam will be only approximately .01 R of the incoming energy, where R is the reflectivity of the sample surface. This contribution is therefore negligible.

The surface temperature measurement is based on the assumption of unit emissivity at a specified wavelength. As shown by previous workers, most silicates have an emittance approaching unity between 7.8 and 8μ. This wavelength interval was used in the data reduction. The error in the assumption of unit emittance has the effect of increasing the relative emittance at longer wavelengths because the color temperature of the sample surface is higher than the temperature arrived at by the computer. This result follows from the fact that in most cases the 8-13μ wavelength region used lies on the shortwavelength side of the energy maximum for the temperature encountered.

No effective method was found to measure the emissivity

of the calibration unit. However, no absolute measurement was necessary for determining relative emittance as long as the emissivity of the unit remained constant with wavelength. A spectrum of velvet paper placed on the sample holder was made to test the emissivity constancy of the calibration device. The maximum departures from unit emissivity were 3%, a value much smaller than for any of the powders measured.

The linearity of the detection system was checked by taking spectra of the calibration device at ice water temperature and dry ice-acetone temperature. The latter spectrum was treated like a sample spectrum, and the resulting temperature computed was 194.8°K. This agreed well with the 194.5°K sublimation temperature of dry ice.

The spectrometer was calibrated using an ammonia absorption cell. The absolute calibration error was a maximum of .05μ and the reproducibility error was .02μ. The measured spectral resolution was .08μ at 9μ.

The peak signal-to-noise ratio varied between 60 and 80, depending on detectors, at a sample temperature of 200°K. This value is the quotient of the output DC signal, at the maximum response of the system, and the rms noise of the detector. To improve the signal-to-noise ratio between two and six spectra were usually averaged. The observed increase in signal-to-noise followed approximately the square root of the number of averaged spectra.

IV. TELESCOPIC OBSERVATIONS

There is good evidence, from several different types of observations, that the lunar surface is not completely homogeneous in its composition.

The most obvious difference would be expected to exist between the composition of the maria and the uplands. The differences in albedo and roughness suggest different textures, alteration or composition, or a combination of the three.

Differences in the magnitude of polarization of the reflected sunlight have been recorded for a number of points on the surface (Dollfus, 1962), although the differences are small (Gehrels et al., 1964).

Small color differences between points on the surface have been reported by many investigators (Coyne, 1963; Petrova, 1966).

Differences in albedo correspond to the borders of major features, such as the maria, and suggest changes in the composition as well as in the physical state.

Thermal anomalies, or so-called "hot spots," were first reported by Shorthill et al. (1960) during an eclipse and have been recorded on the nighttime lunar surface by Murray et al. (1963). These anomalies can be explained by the presence of material having a higher thermal conductivity than the surrounding area. The normally very low thermal conductivity of the lunar surface, determined in the infrared on the basis of eclipse cooling curves (Wesselink, 1948), and supported by microwave emission measurements (Drake, 1966), is

the basis for the belief that a dust layer, probably thin, covers most of the moon's surface.

The choice of positions on the moon for differential 8-13μ spectroscopy was designed to fulfill the following requirements: (1) Measurement of points known from previous work to be anomalous, such as the craters Alphonsus and Aristarchus. (2) Measurement of upland vs. mare differences and ray crater vs. mare differences. (3) Measurement of thermally anomalous areas with the assumption that these areas are partially free of dust and therefore could exhibit greater spectral contrast. The description of the points along with other observational data is given in Appendix III.

4.1 Method

Previous workers in the field of infrared spectroscopy of the moon were hampered by the lack of sensitive detectors for high resolution observations. Even at low resolution the variable transmission and emission of the atmosphere precluded obtaining high accuracy measurements. At night absolute measurements of any kind are difficult to make in the 8-13μ region, because there are no standard bright sources and the atmospheric transmission cannot be accurately determined.

A method for making differential spectral observations of the moon was developed to circumvent these difficulties. This method removes the basic atmospheric absorption and allows the integration of many spectra in order to reduce uncertainties caused by atmospheric absorption fluctuations and detector noise. The details of

the data reduction process are given in Appendix V.

The reststrahlen bands in silicates are generally narrow features varying in width from 0.2μ, in the case of quartz, to 2μ for rock materials. As discussed in Chapter II, the position of these reststrahlen bands in the 8-13μ spectrum is diagnostic of the rock or mineral type. Since the spectral contrast or depth of these lines is small in the emission spectra of powdered materials, it was necessary to develop a method which was sensitive to small departures from graybody emission.

The spectral differences in emissivity between two points 1 and 2

$$\Delta\epsilon(\lambda) = \epsilon_1(\lambda) - \epsilon_2(\lambda)$$

are diagnostic of compositional differences between the two points. However, the value of $\Delta\epsilon$ cannot be obtained directly by remote telescopic measurement. The quantity

$$r = \frac{\Delta\epsilon}{\epsilon_2}$$

which can be recovered from telescopic data, yields similar information to $\Delta\epsilon$ and can be used to determine the wavelength positions of differences in spectral emission which are diagnostic of compositional differences. Using the method discussed below, a value of r as small as .005 in the 8.2-9.2μ and 10-13μ regions and .02 in the 9.2-10μ range can be detected.

The flux density in a wavelength interval $\Delta\lambda$ arriving at the

detector from the lunar surface is given by

$$W(\lambda)\ \Delta\lambda = G(\lambda)\ \epsilon(\lambda)\ B(\lambda, T)\ A(\lambda, t)\ \Delta\lambda \qquad (4)$$

where G is a geometrical factor dependent on the telescope configuration and includes the instrument response, $B(\lambda, T)$ is the blackbody radiance at temperature T, and $A(\lambda, t)$ is the atmospheric transmission which is a function of wavelength and time t.

In order to remove the basic atmospheric transmission component in comparing the spectra of two points, the quotient rather than the difference of two spectra is formed.

$$Q(\lambda) = \frac{W_1(\lambda)}{W_2(\lambda)}$$

Using equation (4) and cancelling terms, the quotient becomes

$$Q(\lambda) = \frac{\epsilon_1(\lambda)\ B_1(\lambda, T_1)\ A_1(t)}{\epsilon_2(\lambda)\ B_2(\lambda, T_2)\ A_2(t)} \qquad (5)$$

The curve $Q(\lambda)$ is composed of several parts:

1. $\frac{\epsilon_1(\lambda)}{\epsilon_2(\lambda)}$, containing the desired information, is a function with a wavelength period short with respect to the complete 8-13μ spectrum.
2. $\frac{B_1(\lambda, T_1)}{B_2(\lambda, T_2)}$ is a slowly varying function of wavelength, as illustrated in Figure 9.
3. $\frac{A_1(t)}{A_2(t)}$ is composed of two parts. One part is a function which has a long wavelength period due to the change in the intervening air mass over the seven minute period of one spectral scan. The second part consists of short-period, random transmission fluctuations. Detector

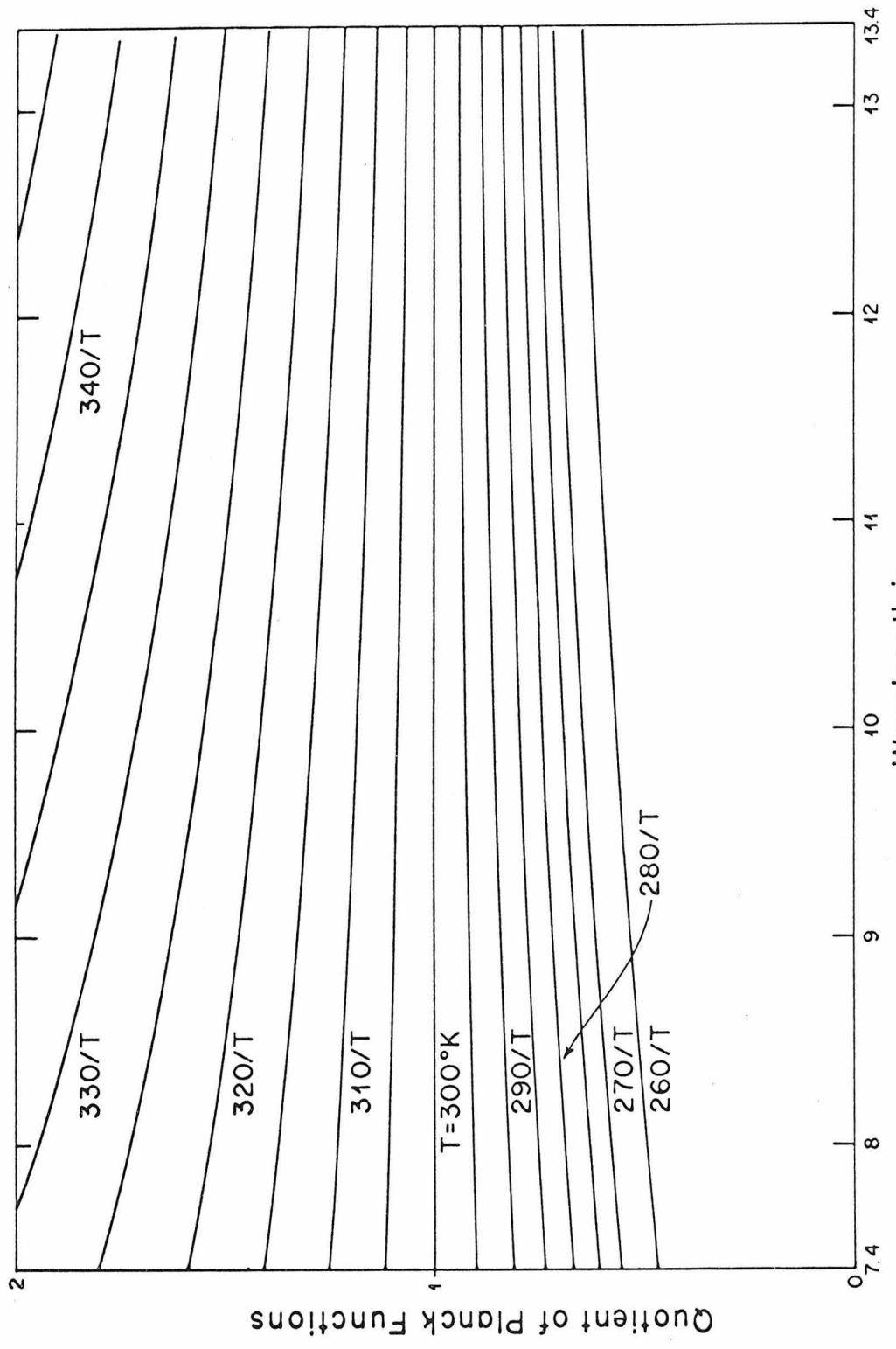

Figure 9. Quotients of Planck functions $\frac{B_1(\lambda, T_1)}{B_2(\lambda, T)}$. T is held constant at 300°K and T_1 is varied from 260 to 345° K in 5° steps.

noise is also random and is made up primarily of high frequency components.

As a matter of convenience in data reduction, the long wavelength period trends had to be removed so that many spectral scans could be averaged to reduce the random noise produced by the atmosphere transmission fluctuations and detector noise. In this process long wavelength period trends in the emissivity difference were also removed.

In order to remove the long period trends in $Q(\lambda)$, a second order polynomial of the form

$$P(\lambda) = a\lambda^2 + b\lambda + c$$

was fitted to $Q(\lambda)$. This is the lowest order polynomial that can be fitted accurately to the quotients of Planck functions. If

$$C(\lambda) = \frac{B_1(\lambda, T_1)}{B_2(\lambda, T_2)}$$

the maximum deviation of $P(\lambda)$ from $C(\lambda)$ is 0.2% for $T_1 = T_2 \pm 20^{\circ}K$ for temperatures ranging from 200° to 400° K.

In the data reduction process, $P(\lambda)$ is fitted to $Q(\lambda)$ by least squares. Since $P(\lambda)$ assimilates all the long period terms, equation (5) can be written

$$Q(\lambda) = \frac{\epsilon_1(\lambda)}{\epsilon_2(\lambda)} P(\lambda)$$

and the residual is then defined as

$$r = \frac{Q(\lambda) - P(\lambda)}{P(\lambda)}$$

The residuals r calculated from pairs of spectra taken at different lunations can be compared and averaged to reduce the effect of atmospheric and detector noise.

Figure 10 demonstrates the effectiveness of this integration process. The upper curve represents the average of the data residuals of the quotients of ten pairs of spectra taken of the same spot in Mare Tranquilitatis. Ideally these residuals should average to zero. The departures from zero represent the failure of the integration process to eliminate the short period noise components completely. This curve then represents the level of confidence in the data obtained from spectra of an adjacent point and the point in question. In Figure 10 the adjacent point is the center of Mare Serenitatis. The residuals of this quotient of Mare Tranquilitatis and Mare Serenitatis are given in the center curve. The lower curve again represents the confidence level in the data making up the center curve.

In spite of the fact that the center curve represents the quotient residuals of two different lunar positions and r is not expected to be zero, fluctuations are less than in the confidence curves above and below it. This result demonstrates the power of the integration technique and the absence at this level of systematic error caused by coherent noise. In this case, for the average of twenty-three pairs of spectra, spectral emissivity differences between areas on the moon can be detected which are as small as 0.005 in the 8.2-9.2μ and 10-13μ region and 0.02 in the 9.2-10μ range. Under excellent observing conditions fewer integrations are required to attain this sensitivity.

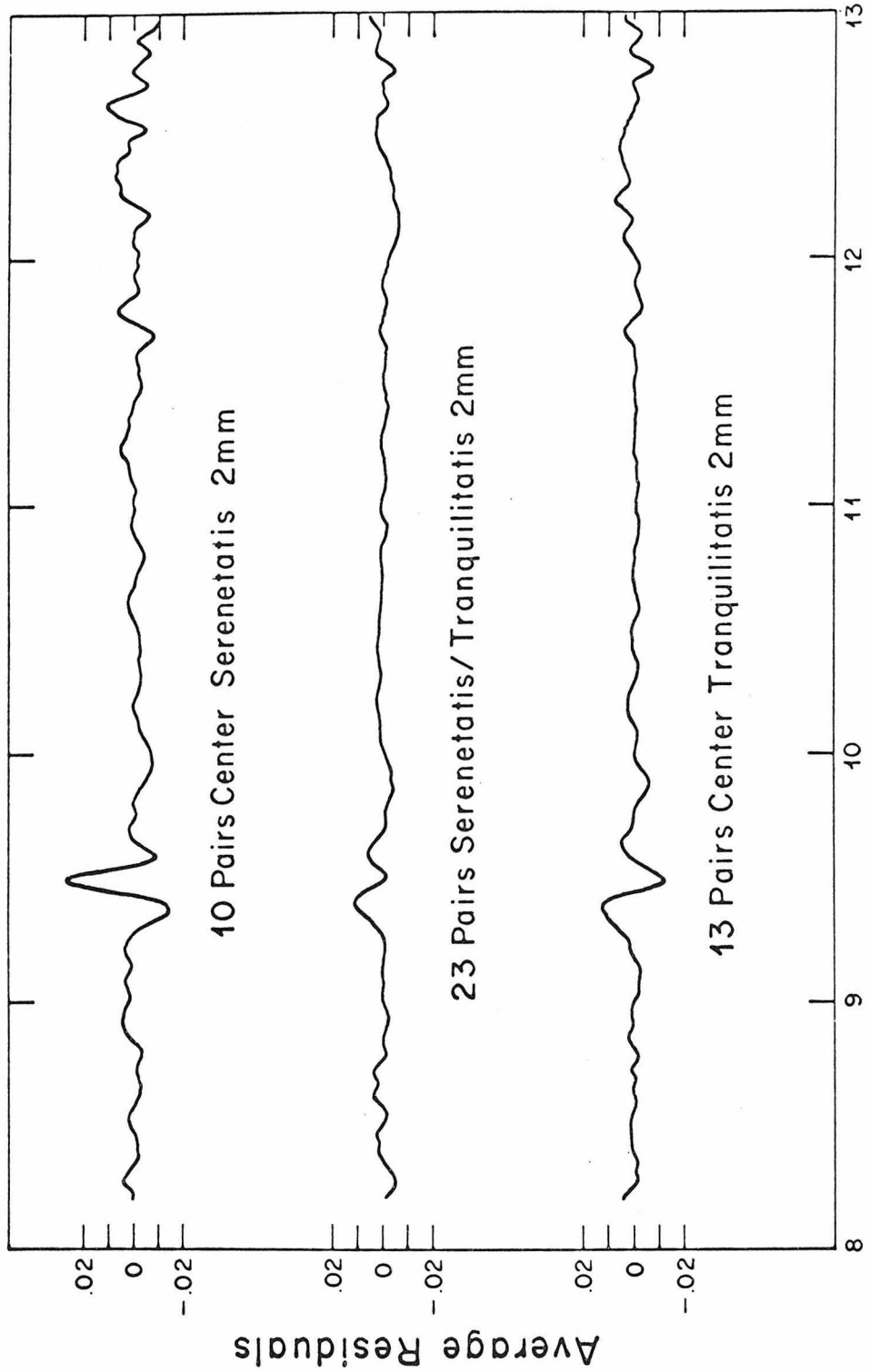

Figure 10. Average residuals for two lunar areas. The upper and lower curves represent pairs of spectra taken of the same point. The center curve represents the comparison of spectra taken alternately of each point.

The region between 9.2 and 10μ is excluded when making the second-order fit to the quotient in order to prevent biasing the residuals with the use of data from this region of poor signal-to-noise ratio. The possible causes for the data being poor in this wavelength region are discussed in Section 4.4.

The method described above is applicable for detecting emissivity differences which have a wavelength period of less than about 2μ and greater than 0.1μ. This is adequate for detecting emissivity changes due to mineralogical differences between two points on the moon.

The possibility of long period variations in $\Delta\epsilon$ over the entire 8-13μ region still remains. The above process would obliterate such long period changes by absorbing them in the fitted polynomial.

To investigate such possibilities, the fitted polynomials were used instead of the actual quotients of the spectral scans. As discussed above, the polynomials absorb slow variations in the atmospheric transmission due to changes in air mass. In order to obtain a polynomial free of atmospheric bias, quotient fits of pairs of spectra from two points taken in opposite order in time were averaged. In practice spectra were taken of the points A and B in the sequence A_1, B_1, A_2, near the meridian where the change in air mass was nearly constant. The quotients A_1/B_1 and A_2/B_1 were formed.

Assuming a temperature T_B calculated from the visible albedo and the sun's elevation angle and the solar constant, a T_A can

be found in the expression for $C(\lambda)$ which gives a best fit to the average quotient. The differences in the two curves correspond to long wavelength period emissivity variations between the two points on the lunar surface. Figure 11 shows a plot of the two quotients for Mare Tranquilitatis vs. Mare Serenitatis, their average and the closest fitting quotient of Planck functions $C(\lambda)$. The differences between the average quotient and $C(\lambda)$ are everywhere less than 2%. The assumed T_B was 383°K and the calculated T_A 371.3°K.

4.2 Instrumentation

The lunar observations were carried out with a 24-inch reflector on Mt. Wilson. The bent cassegrain f16 focus was used, which has a plate scale of approximately 20 sec. arc/mm. The two-beam photometer used was the same basic device described by Westphal et al. (1963). A modified Ebert-Fastie grating spectrometer fitted with a mercury-doped germanium detector was mounted on the photometer. The difference signal of the beam focused on the moon, and the adjacent sky beam was amplified and synchronously detected. The output signal was recorded simultaneously on a strip chart recorder and on paper tape in digital form. Three circular entrance apertures 2, 1.5 and 1 mm in diameter were used. A more detailed description of the instrumentation is given in Appendix IV.

4.3 Procedure

Data from 22 lunar positions were collected on 43 nights in 1966. A total of 794 spectra were recorded. This number includes about seventy-five spectra taken for calibration and testing. The

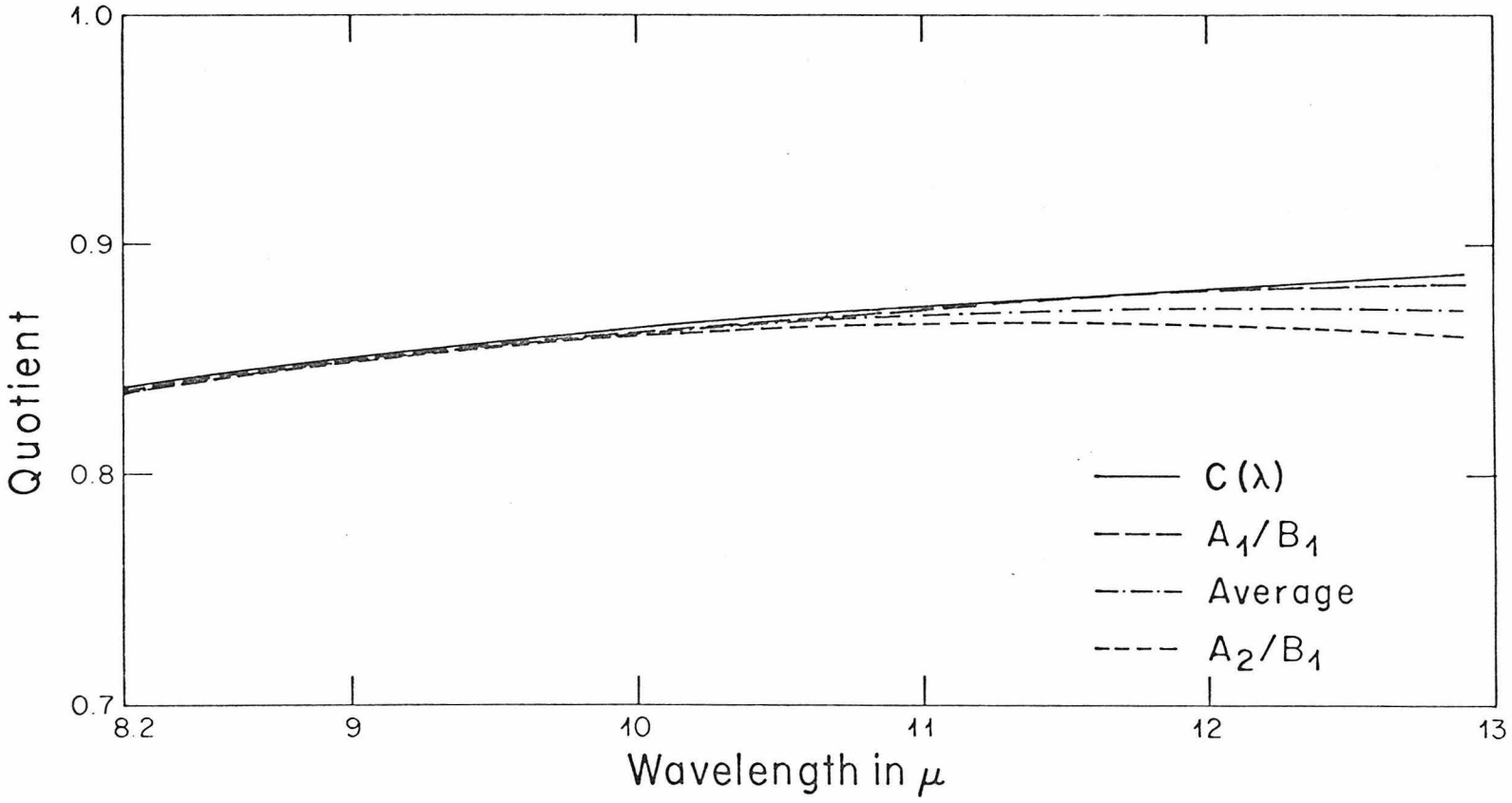

Figure 11. Curves showing the long wavelength period emissivity difference behavior between the points Mare Tranquilitatis (A) and Mare Serenitatis (B).

first 160 spectra were excluded from the final analysis because of instrument calibration inaccuracies.

Two procedures for data acquisition evolved during this period. The first procedure was aimed at covering as many different points of interest on the moon as practical. Two "traverses," or loops were set up, one on the eastern half and one on the western half of the lunar disk. These measurements were made with the highest spatial resolution possible (20 sec. arc) commensurate with adequate instrumental signal-to-noise ratios. Spectra were obtained from the eastern loop, beginning two days after first quarter and continuing until two days after full moon. Measurements were made on the western loop, beginning two days before full moon and ending two days before third quarter.

Two consecutive spectra were taken at each point. A total of fifteen minutes was required, which included one minute of re-setting the wavelength counter, labeling the digital record and repositioning on the object between scans. The time required to acquire a new lunar position was usually less than one minute.

The second procedure evolved from the first one and was used to tie in the two loops and make more detailed studies of individual lunar positions. Two consecutive spectra were taken at each point until the moon neared the meridian. Spectra were then taken alternately of each of the two points, in order to acquire data for measurements of the long period changes in $\Delta\epsilon$. Larger apertures were used for mare areas and large craters in order to increase the

signal-to-noise ratio. Figure 12 shows the lunar positions observed. Lines connect the positions measured consecutively. The diameters of the circles represent the aperature sizes used.

4.4 Error Analysis

There are a number of sources of error, both in the collection of data and in its analysis. The principal sources are: (1) atmosphere, (2) telescope, (3) spectrometer, (4) detector, (5) amplifier, (6) digitization, (7) data reduction method.

Atmospheric emission and transmission fluctuations are the chief sources of error introduced into the system. The emission from the atmosphere as well as from the telescope is cancelled out by the use of the two-beam photometer. In practice both beams are pointed at the sky, and the sky beam is adjusted so that the output difference signal is reduced to zero at the peak response of the system. The maximum DC component originating from incomplete cancellation of the sky emission is less than 1%. Since this component is additive in each spectrum, the error in the quotient is reduced by an order of magnitude. The balance of the beams requires no adjustment during a night's run.

The variations in atmospheric emission affect the signal-to-noise ratio in inverse proportion to the signal strength. Observations of the output signal when both beams are on the sky show that, on a good night, emission noise is equal to or less than detector noise.

The atmospheric transmission fluctuations are more critical, since they cannot be reduced by increasing the signal level at the

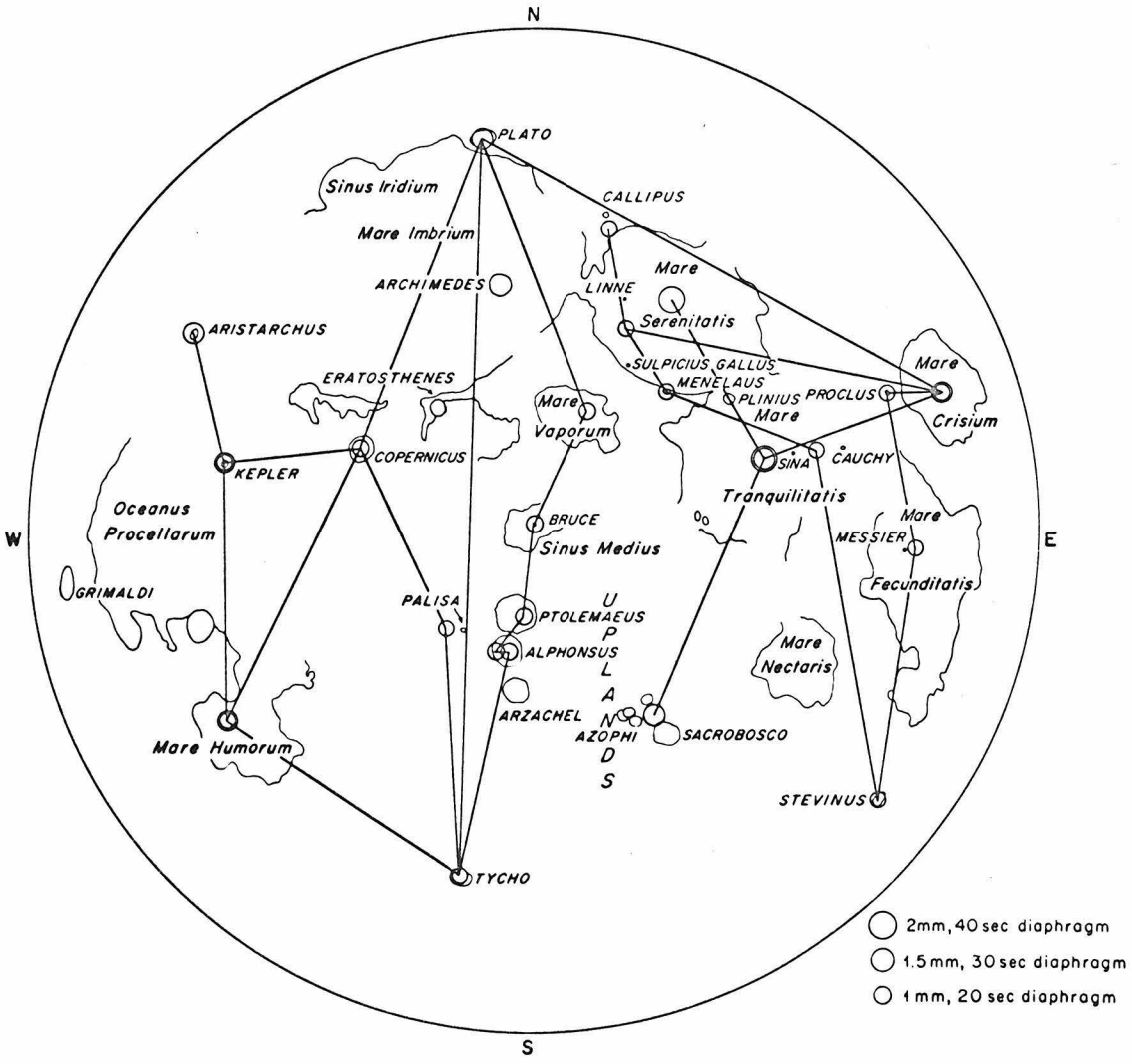

Figure 12. Lunar positions observed during the investigation. Lines connect the positions measured consecutively. The diameter of the circles represent the aperture sizes used.

detector. The amount of transmission noise is extremely variable, sometimes changing abruptly during a night's run. Short period variations (1-minute time scale) average about 2%. However, under poor conditions without any visible clouds, the transmission was occasionally observed to change by as much as 10% over a one-minute period.

The telescope is equipped with lunar drive rates, which make it possible to guide on one position quite accurately. The maximum deviation in guiding was one-half an aperture diameter. Since the temperature variations are small about a lunar position fully illuminated by the sun, the signal fluctuations caused by guiding errors were small. In a seven-minute period the measured variations due to guiding errors on the crater Copernicus were less than the atmospheric noise. A similar experiment carried out on Mare Serenitatis produced the same results.

The absolute wavelength calibration of the spectrometer was accurate to .05μ. The reproducibility was better than .02μ in all cases. This reproducibility was adequate for all wavelength regions except the 9.2-10μ ozone band. The steep slopes of the ozone band introduce an error into the quotient of two spectra if data points are not taken at exactly the same wavelength in each case. The wavelength reproducibility error contributes to the poor accuracy in this region. The lower signal levels and corresponding decrease in the signal-to-noise level are also contributing factors.

The cooled mercury-doped germanium detector is basically

a photon detector and is therefore a highly linear device. No non-linear response was observed in the ranges of intensity used. Current noise produced in the detector was a major source of uncertainty in the data. Signal-to-noise ratios at peak response varied from 60, using a 1mm aperture at quarter phase, to 1500 for a 2mm aperture at full moon.

The amplifier used had a linearity of better than 1% above a 5% scale deflection. Spectra were always taken at the same amplifier gain setting. Amplifier noise was less than 0.1% of the detector noise. The 24-inch telescope is located on a ridge approximately one-quarter mile east and in full view of the large Mt. Wilson TV and FM transmitting facilities for the Los Angeles area. In spite of shielding precautions, some RF noise pulses appear in the data. The interference problem is most noticeable when the moon is observed in the western sky and the dome is open to the direction of the transmitting antennas.

The digitizer has an accuracy of .01% of full scale and displays four significant figures.

The errors and accuracies discussed above apply to the collection of data. The errors introduced by data reduction, insofar as they have not been previously mentioned, are discussed in Appendix V.

4.5 Observational Results

Figure 13 is a composite of the average residuals for the eastern loop. Beginning with Sulpicius-Linne, the points alternate

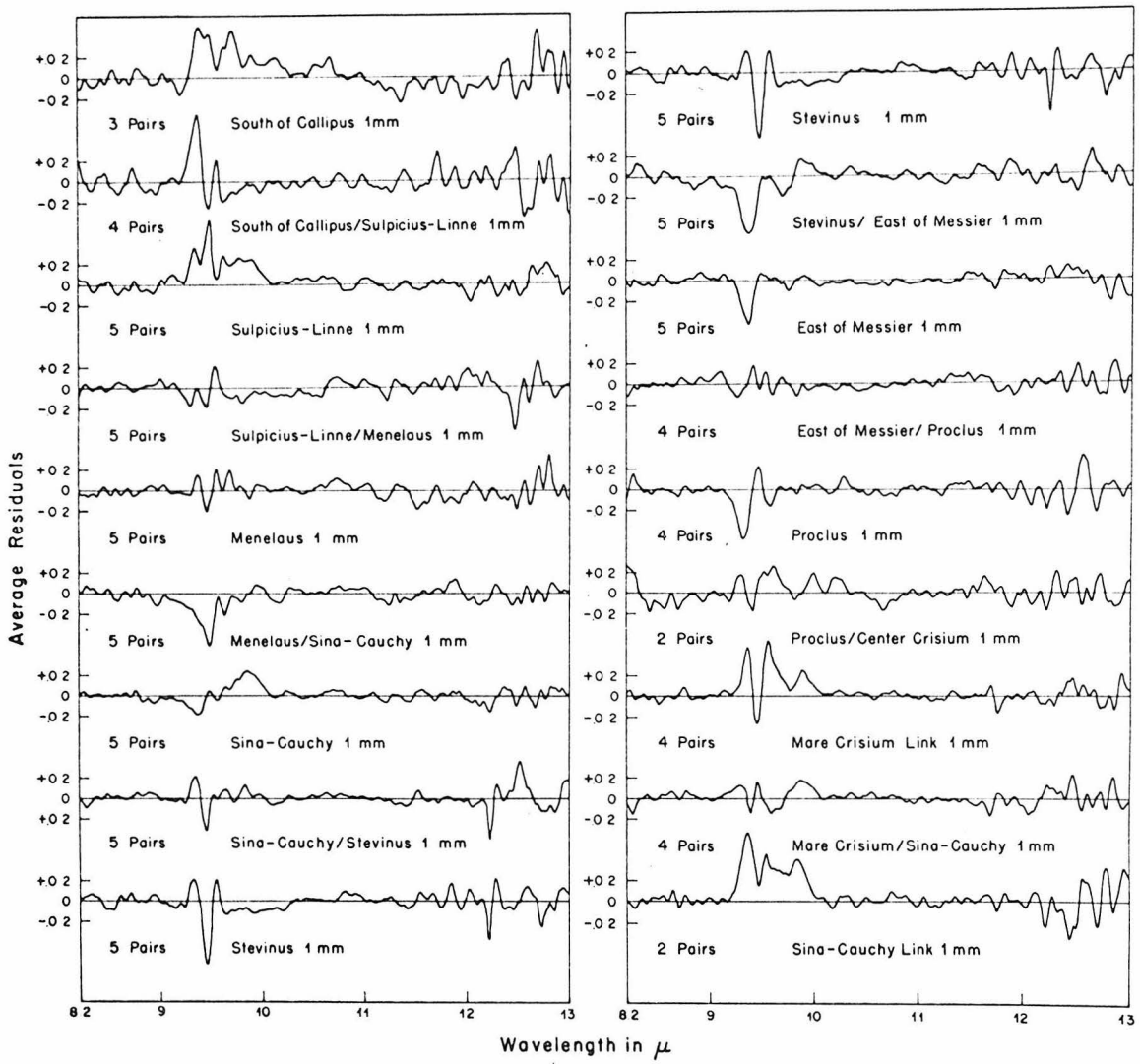

Figure 13. Average residuals for the eastern loop.

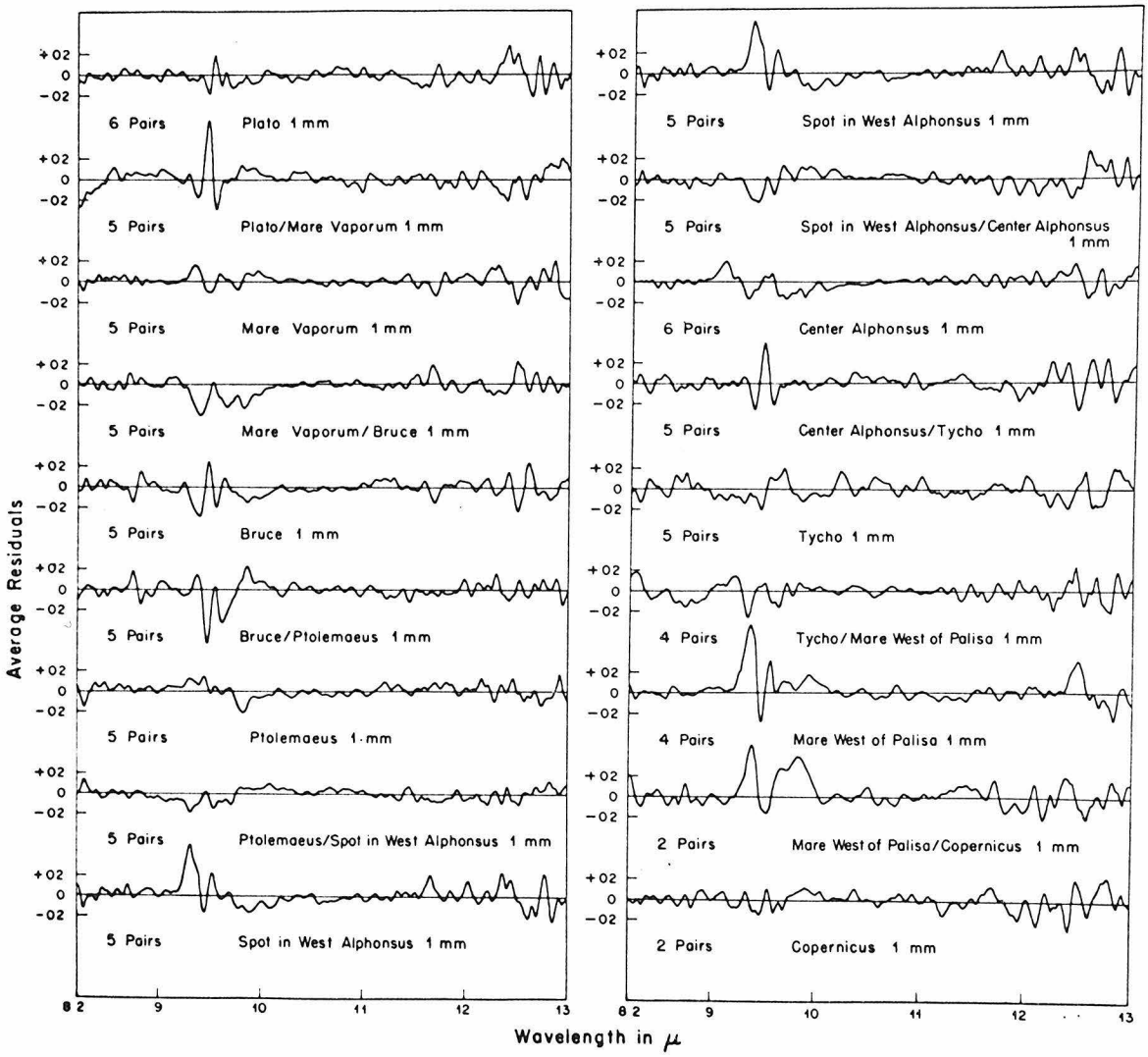

Figure 14. Average residuals for the western loop.

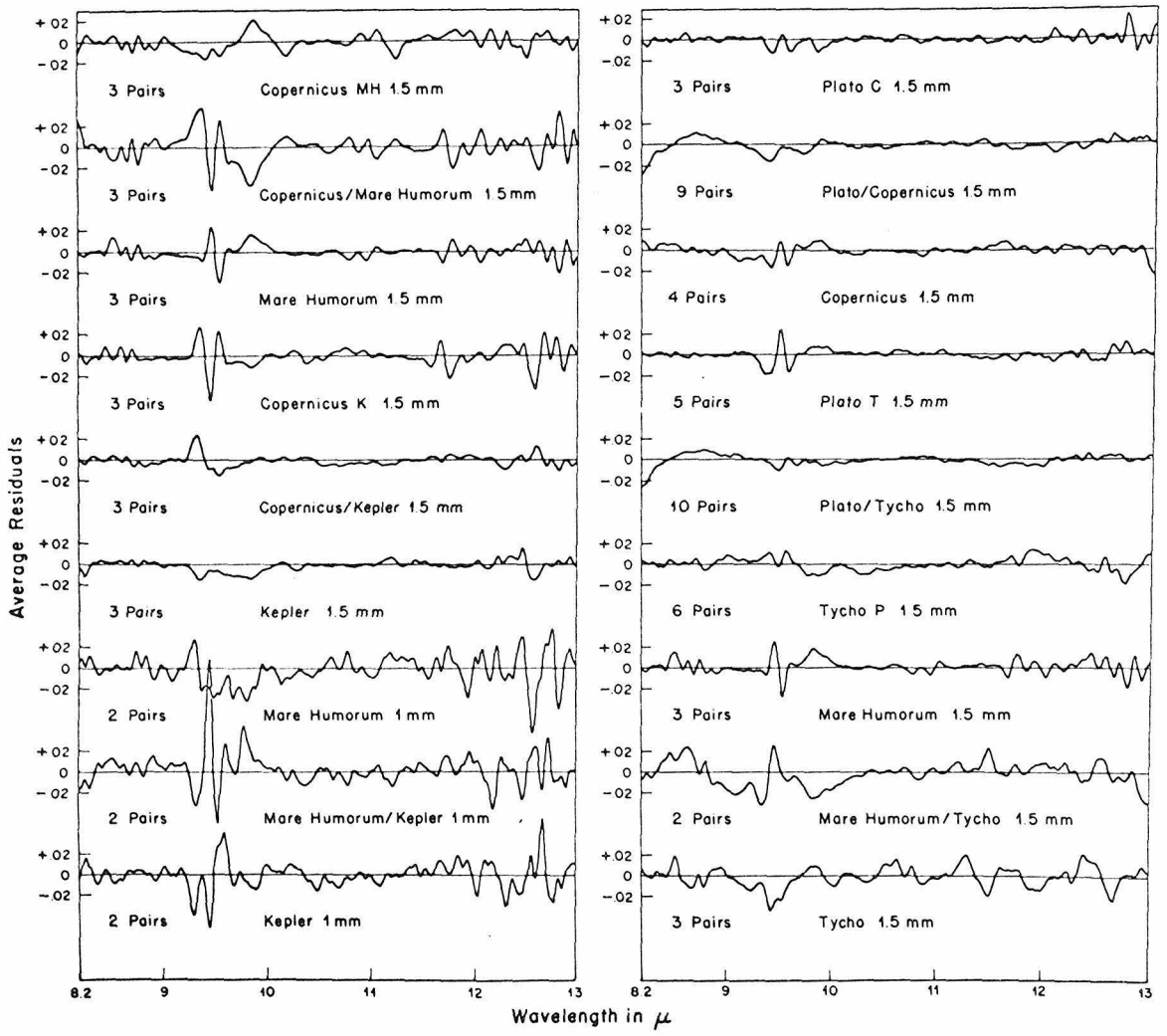

Figure 15. Average residuals for some of the individual sets of measurements not carried out on a loop.

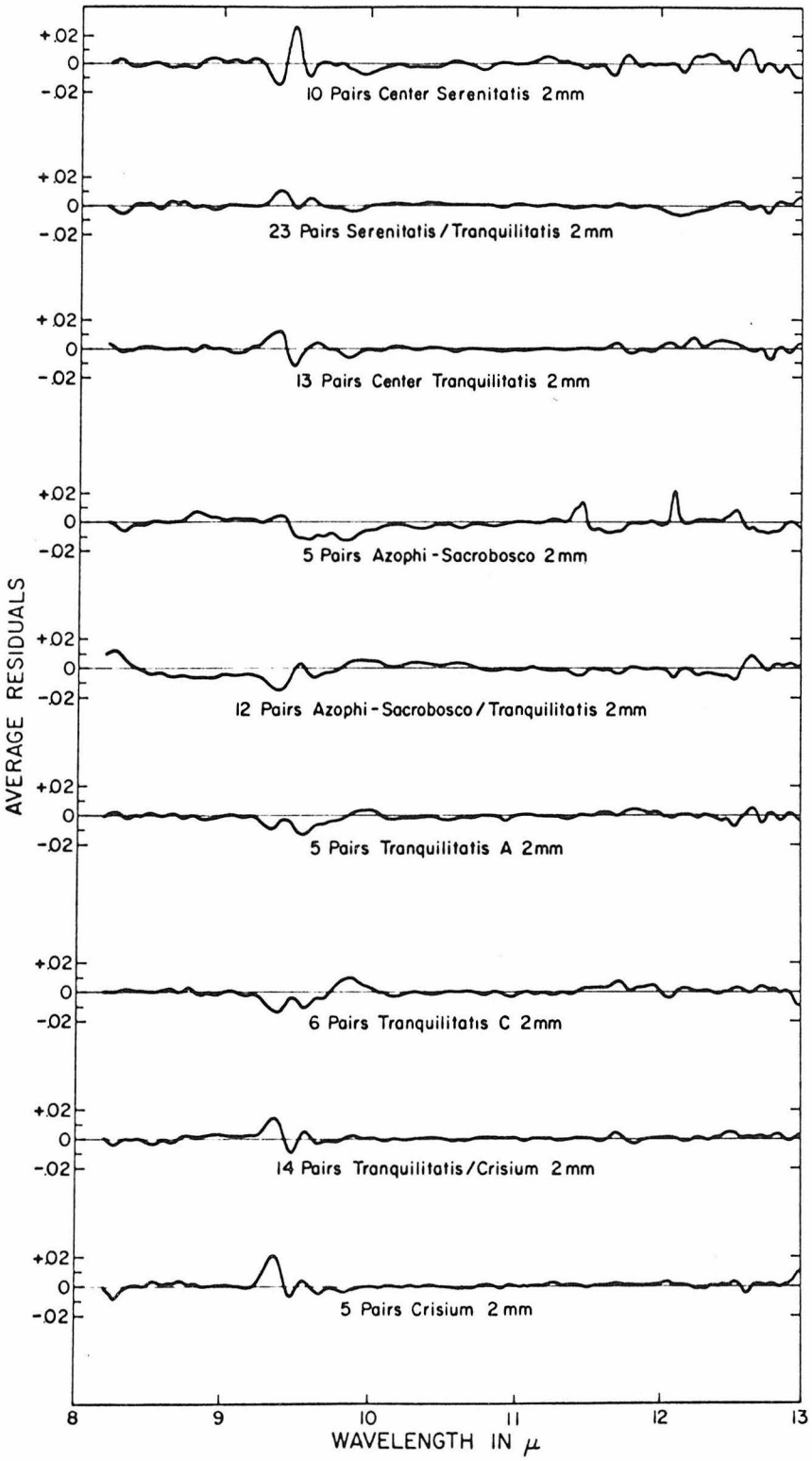

Figure 16. Average residuals for points taken with the large aperture and incorporating a large number of measurements.

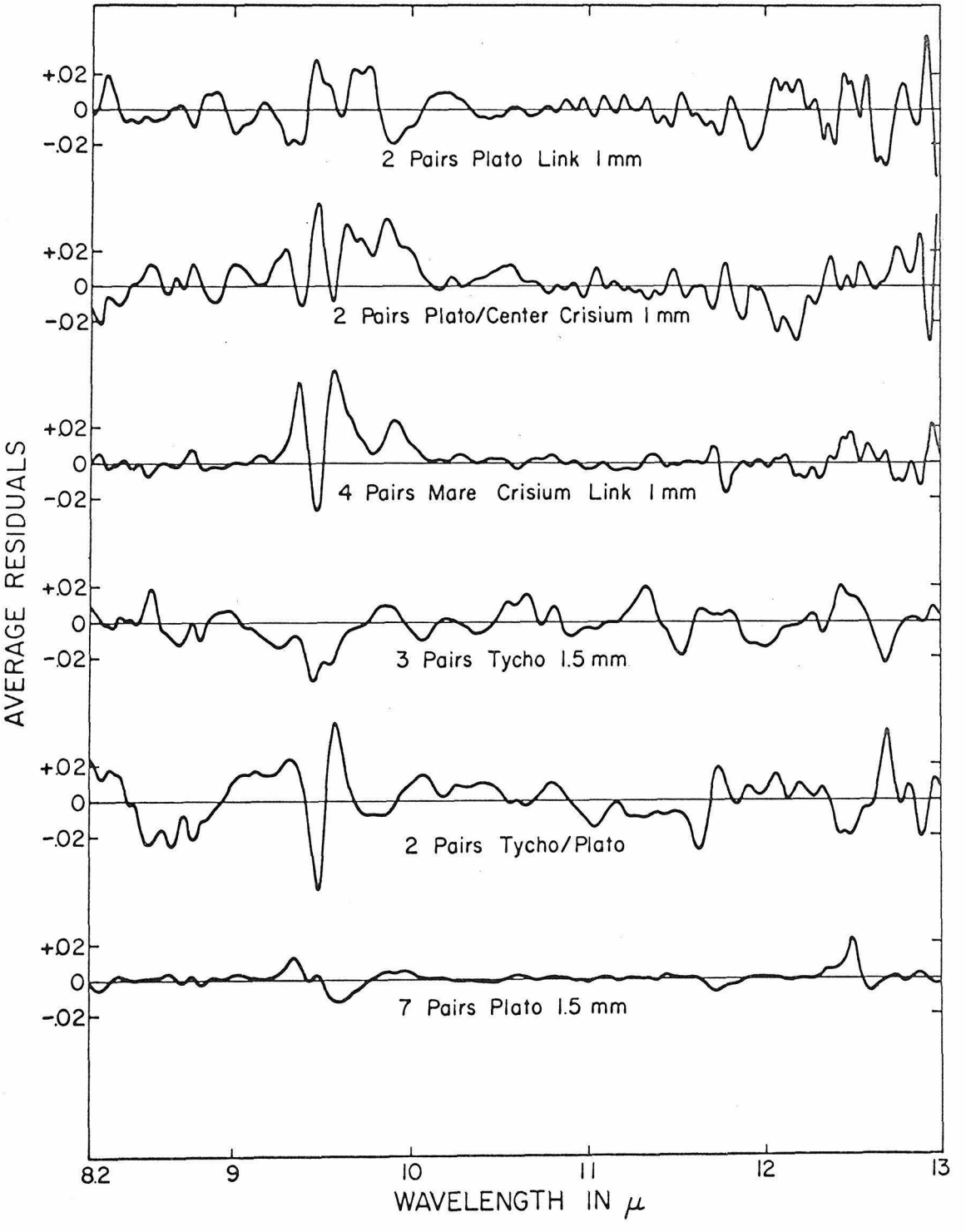

Figure 17. Average residuals showing the behavior of the emissivity of Plato between 8.2 and 8.4μ.

between mare regions and bright ray craters. "South of Callipus" is on the border of Mare Serenitatis. The residual curves having one position name are understood to be the quotient residuals of that position versus itself. Ideally these curves should be straight lines through the zero point, as discussed in Section 4.1.

All the curves exhibit noise fluctuations, although outside the region 9.2 to 10μ those fluctuations average $\pm$ 1% or less. Within the level of confidence given by the quotient residuals of the individual positions, there is no significant departure from zero for any of the residuals shown in this figure.

Figure 14 is a similar composite for the western loop. In the left half of the figure the only significant departure from zero is seen in the Plato/Mare Vaporum curve between 8.2 and 8.6μ. The emissivity of the Plato surface varies from 0 to 2.5% lower than the surface of Mare Vaporum. The previous statements can also be written: the emissivity of the Mare Vaporum surface varies from 0 to 2.5% higher than the surface of Plato, because of the sign ambiquity inherent in the differential measurement. The term emissivity is being used loosely here and the assumption is made that $r \approx \Delta\epsilon$. However, comparison spectra of subsequent points in the loop show no differences in this wavelength region.

In the right half of the figure the curve Tycho/Mare East of Palisa exhibits departures from zero, both positive and negative, in the region 8.2 to 9μ. However, the low confidence level shown by the curve Tycho in this region makes the validity of these departures

uncertain.

Figure 15 is a collection of residuals representing individual sets of measurements not carried out on a loop. Mare Humorum is compared individually with three other areas: Copernicus, Kepler and Tycho. In each instance it is seen that Mare Humorum has a lower emissivity between 8.2 and 8.4μ. There is some indication that Mare Humorum has a higher emissivity than the comparison points between 8.4 and 8.8μ. However, this is only obvious in the Mare Humorum/Tycho curve.

The two curves yielding the strongest evidence that the lunar surface is not completely gray are Plato/Copernicus and Plato/Tycho. The similarity between the two is striking. The main features are the departures of r from zero between 8.2 and 9μ. The lower emissivity for Plato between 8.2 and 8.5μ is consistent with the Plato/Mare Vaporum and Plato/Mare Crisium curves.

Figure 16 shows curves incorporating a large number of measurements. Azophi-Sacrobosco was taken as a typical uplands point. No significant difference between this uplands point and Mare Serenitatis is apparent. The remaining curves also do not exhibit significant departures from zero.

The two sets of curves in Figure 17 give additional evidence of the decreasing emissivity of Plato in the 8.4-8.2μ region. Plato/Center Crisium is the link between the eastern and western loop of data points. The Tycho/Plato curve is based on a set of measurements not included in the Plato/Tycho curve in Figure 14. The signs

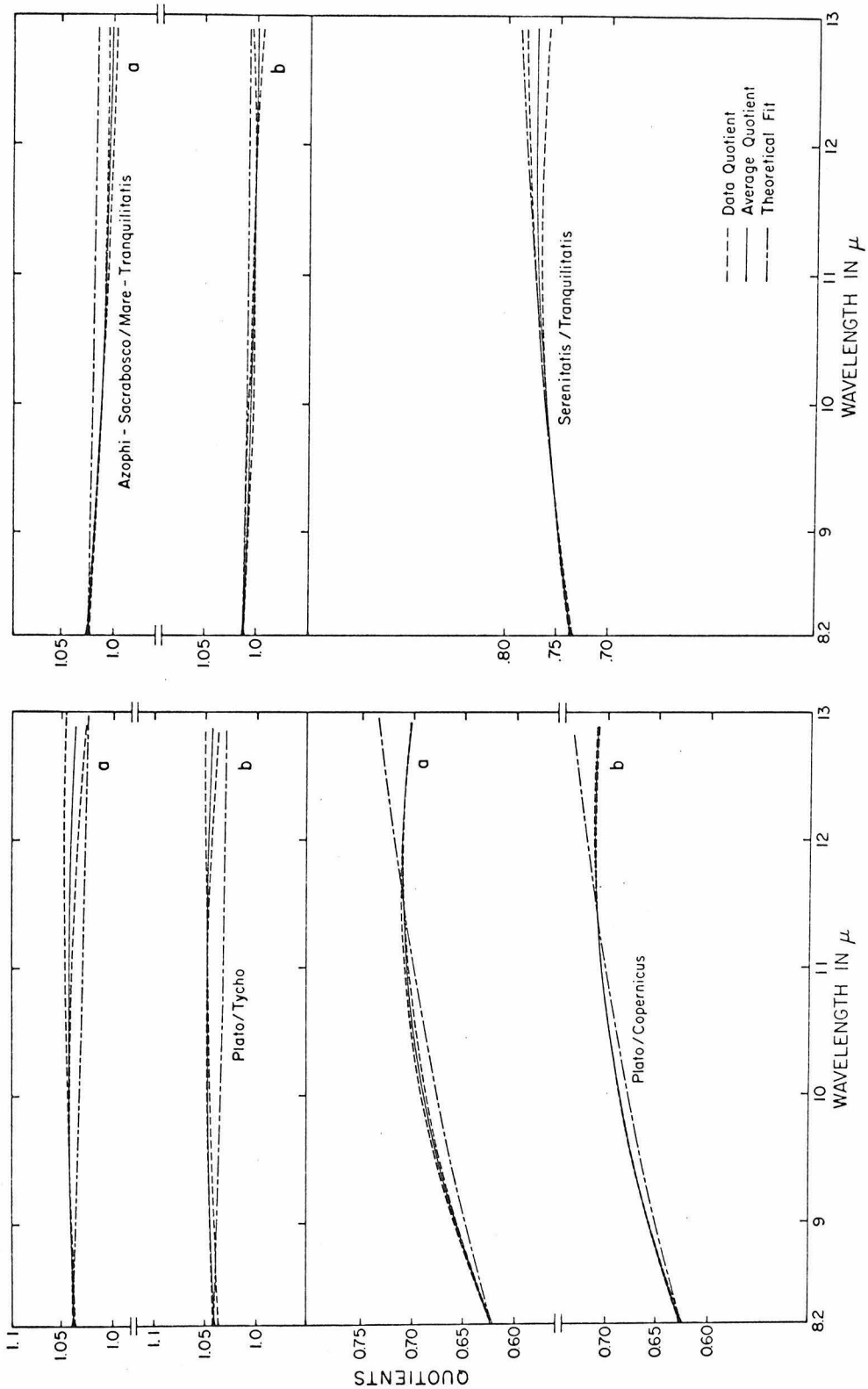

Figure 18. Fitted polynomials and theoretical quotients C(λ) showing the long wavelength period behavior of the emissivity difference.

of the emissivity differences in the 8.2-9μ region agree in both curves, although the curve in Figure 16 shows a much lower level of confidence.

The results of the comparison of the fitted polynomial quotients and the theoretical quotients discussed in Section 4.1 are shown in Figure 18. Each set of curves is composed of data from three spectra of two lunar positions, A and B, taken in the sequence A_1, B_1, A_2. The dashed lines represent the polynomials fitted to the two quotients, A_1/B_1 and A_2/B_1. The solid curve is the average polynomial and is presumably unbiased by slow changes in atmospheric transmission during the spectral scans. The theoretical curve is the quotient of two Planck functions. The theoretical and average quotients are arbitrarily fitted at the short wavelength end of the spectrum.

The vertical scale has been greatly expanded to show small differences. In the case of the Plato/Tycho curves the maximum deviation of the average quotient from the theoretical quotient is 1.2%. The greatest difference among all the curves is 4.1% at the long wavelength end of Plato/Copernicus.

The only possibly significant difference in the shape of the average and theoretical curves is found in Plato/Tycho. The shape or curvature of the quotient of two Planck functions is very insensitive to temperatures in the range of lunar surface temperatures in this wavelength region. A change of $\pm 30^{\circ}K$ in the assumed temperature for T_B would not noticeably affect the shape of the quotient.

Of course, a different T_A would be needed to match the theoretical quotient with the average quotient.

V. CONCLUSIONS

Analysis of 8-13μ difference spectra of 22 points on the lunar surface has revealed two facts: (1) Twenty of 22 points, including all major types of surface features, showed no spectral contrast greater than 1%. (2) Two points, Plato and Mare Humorum, showed definite, consistent spectral differences from the rest of the points measured, at the short wavelength end of the spectrum.

Previous measurements by Hunt and Salisbury (1964) in the 16-24μ region showed spectral differences amounting to as much as 10% between Copernicus and Serenitatis. Smaller spectral differences were recorded for Tycho and an uplands point. Hunt et al. (1966) report average differences of 1 to 2% between Mare Tranquilitatis and Mare Serenitatis over a wide range of wavelengths extending from 7 to 24μ. Differences of these orders of magnitude were not detected in the present investigation. In the 8-13μ region, differences were less than 0.5% between Serenitatis and Tranquilitatis.

The 16-24μ measurements by Hunt and Salisbury were made using a single-beam instrument. No attempt was made to remove the effect of the variable atmospheric transmission or emission, nor were the measurements always reproducible (Salisbury, private communication). The method used by Hunt et al. was lunar temperature dependent, although an attempt was made to circumvent this difficulty. However, the authors did not make an error analysis, which leaves the validity of their data open to question.

Differences in the emission spectra of the points observed were expected for several reasons. (1) A variety of lunar surface features, including uplands, maria, bright ray craters and a black halo crater was represented in the points measured. These features span the entire range of observed albedos on the lunar surface. Compositional differences between such features have been suggested to explain the different visible albedos. (2) Features having different ages were also represented. Bright ray craters are younger than the surrounding material, as shown by the sequence of deposition of the ejected material. (3) Surveyor I photographs (Jaffe et al., 1966) show a surface made up of generally unsorted material with a uniform size distribution down to the resolution limit of 1 mm. Van Tassel and Simon (1964) reported spectral contrast in a spectrum of olivine flour with an average grain-size of 20 microns, containing a few large grains approximately .1 mm in size. In spite of the fact that there probably is a large amount of fine-grained material on the lunar surface, some spectral contrast is expected. (4) The spatial resolution was high enough so that the observed areas were almost always within a region of uniform albedo. Therefore the averaging effect due to many rock types in the field of view was not expected to be significant. In as much as most of the observed features do have uniform spectra, some process which does not affect the visible appearance of the lunar features and is independent of the age of the feature must therefore be causing spectral homogeneity in the 8-13μ wavelength region.

There are two possible mechanisms for the above process. (1) Microscale roughness of the surface is obliterating the spectral contrast, regardless of composition. (2) Radiation effects of an unknown nature have destroyed the spectral contrast.

Uniform microscale roughness could be the reason for the observed spectral homogeneity. Rock surfaces roughened on a micron scale, as well as micron-sized dust particles, give rise to contrast-free emission spectra. McCracken and Dubin (1963) have discussed the expected high influx of dust particles on the moon's surface. The rounded appearance of bounder-sized material in Surveyor I photographs is probably the result of micrometeorite erosion. The boulder surfaces can be expected to be roughened on a micron scale, since the micrometeorite bombardment removes material by cratering.

Radiation damage or contamination, as discussed in Section 3.3, is another possible reason for the absence of spectral features. Hapke (1965, 1966) is able to match the moon's photometric properties very well with hydrogen-ion-irradiated dunite powder having a particle size of 7 microns. Other materials were also irradiated and were darkened to an extent dependent on the level of exposure. According to Hapke, the non-stochiometric compound formed by sputtering caused the samples to appear redder and to fit more closely the visible reflecting properties of the moon than did the unirradiated powders. Any coating which is optically thick in the 8-13μ region would completely disguise the nature of the coated material.

Very recently Greer and Hapke (1967) reported that electron microprobe analyses of low-energy ion-irradiated materials gave evidence of foreign contamination, causing the reported darkening effects, and therefore cautioned against extrapolating the effects of the irradiation process to extraterrestrial conditions. The actual effect of the solar wind on the spectral contrast is unknown at this time. However, it must be considered a probable factor in producing the homogeneous character of the lunar spectral emission, because it affects the lunar surface in a uniform manner.

The two features which showed spectral contrast with respect to the rest of the observed points were Plato and Mare Humorum. The emissivity differences are similar in character in both cases and show a decreasing emissivity between 8.4 and 8.2μ.

Two other points, Copernicus and Tycho, for which there exist excellent difference spectra with respect to Plato, showed a lower emissivity between 8.4 and 9μ. This departure does not consistently appear in the comparison of Copernicus and Tycho with other features. Although Tycho-Mare West of Palisa and Mare Humorum/Tycho are consistent with a decrease in the Tycho emissivity between 8.4 and 9μ, Center Alphonsus/Tycho and Mare West of Palisa/Copernicus are not. Further discussion is therefore based only on the decreasing relative emissivity of Plato and Mare Humorum between 8.4 and 8.2μ as compared to the remainder of the lunar localities.

Historically Plato has been the subject of many reports of

sightings of bright spots, red spots and total obscurations. Middlehurst and Burley (1966) have compiled a list of lunar events which shows that as long ago as 1685 visible anomalies have been reported in and around Plato. Mare Humorum was not mentioned in the Middlehurst and Burley compilation. However, this mare was reported by Shorthill and Saari to be "thermally enhanced." This means that during the penumbral phase of a lunar eclipse Mare Humorum remained at a higher temperature than its surroundings. Drake (1966) reports an anomalously low microwave temperature for Mare Humorum consistent with the postulate that this region has a low average emissivity. Plato, on the other hand, shows no signs of hot spots or thermal enhancement.

Plato does not exhibit any special features to the visual observer. It appears to be an older, partially filled crater. The surface is smooth and exhibits some light streaks of ray material with an external origin.

Mare Humorum does exhibit some peculiar features. The most striking features are the large concentric rilles on the east and west margins. The mare floor contains numerous wrinkle ridges and several small ray craters. However, the point measured did not coincide with any of these features. Salisbury et al. (1965) discuss the possible origin of the different Mare Humorum structures.

It is difficult to imagine a model in which Plato and Mare Humorum are not subject to the same average solar wind flux and dust bombardment as the rest of the lunar surface. Therefore,

either these areas (1) have significantly fresher surfaces exposed which still show some spectral contrast, or (2) they are mineralogically different than their surroundings, or both.

If all the homogeneous points are considered to be graybody radiators and the two anomalous points have fresh surfaces with spectral contrast, then a material must be found which has the characteristic or decreasing emissivity between 8.4 and 8.2μ. A thorough search of the literature does not reveal any silicate material which has this characteristic. In general, silicates exhibit an increasing emissivity in this wavelength region, with acidic rocks having a much sharper increase than basic rocks because of the proximity of the 8.5 to 9μ quartz reststrahlen bands. Therefore the fresh surface exposed cannot consist of a rock forming silicate material known on the earth. A sublimate is suggested as a possible surface material. Emission spectra of such materials have not been published. However, characteristic absorption curves for inorganic anions have been published by Miller et al. (1952). Carbonates, nitrites and nitrates exhibit reststrahlen bands in the 7-8μ regions, while phosphates and sulfates have characteristic bands in the 8-13μ range.

On the other hand, if the anomalous points have a different composition from the rest, and if the homogeneous points exhibit a lack of spectral differences because they are mineralogically similar but do exhibit spectral contrast, then it must be concluded that Plato and Mare Humorum have a more basic composition than the homogeneous points. The emission spectra of the surrounding

homogeneous points must then contain quartz or SiO_2 glass reststrahlen bands to produce such an abrupt change in emissivity.

There would be, of course, far-reaching implications coupled with the possible existence of quartz on the lunar surface. The presence of quartz would imply some sort of mineralogic phase differentiation process during the development of the lunar crust, since quartz is not an abundant material in meteorites or in any other material postulated for the composition of the primoidal moon.

In summary, most of the regions of the moon surveyed appear homogeneous in their 8-13μ spectral emission. Since a wide variety of visibly quite different features, both young and old, are represented in this group, some mechanism which is responsible for the obliteration of infrared spectral contrast acts more quickly than the mechanism which reduces the contrast of visible structural features. The most likely explanation would appear to be the roughening of the surface by micrometeorite bombardment, although radiation effects cannot be ruled out.

The fact that areas exhibiting infrared spectral contrast do exist, points to a process which operates on a shorter time scale than the obliterating effect discussed. This process is apparently independent of aging rates since Plato and Mare Humorum do not visually appear to be younger than other lunar features.

If this process is producing a fresh surface at these points and the rest of the features have no spectral contrast some non-silicate must be present on the fresh surface to account for the

emissivity behavior. However, if the homogeneous points are compositionally similar and exhibit spectral contrast, then they must contain quartz and have a more acidic composition than Plato or Mare Humorum.

Plato and Mare Humorum are probably not the only anomalous features on the moon's surface. Further observational work is necessary to find more anomalous points and possibly obtain some correlation with visible observations so that a more specific model can be postulated.

APPENDIX I. LABORATORY INSTRUMENTATION

Apparatus

The present system is based on an earlier instrument designed for measuring the thermal conductivity of powders in a vacuum (Watson and Bauman, 1963) but was altered considerably for the sake of cooling efficiency and compactness (Goetz and Bauman, 1967).

Figure 19 shows a cross-sectional view of the chamber. The main parts comprising the system are: (A) The outer chamber wall; (B) the annular dewar or shroud with a capacity for one liter of liquid nitrogen; (C) the combined constant temperature bath and sample holder; (D) cold diaphragms; (E) the calibration device; (F) the chopper; (G) the phase detector; (H) the magnetic drive assembly; (I) the BaF_2 window. The entire chamber and its contents except for the calibration device and chopper were constructed of stainless steel. The annular dewar is supported only by J, the fill tube, at the top and K, three knife edge nylon supports, at the bottom, directly above the sample holder. This shroud provides a cold half-space into which the powder surface radiates. It was filled automatically at thirty minute intervals from a 25 liter storage dewar by a simple clocked timed heater contained in it. The consumption under normal operating conditions was 25 liters in twenty-four hours.

The constant temperature bath is supported on the base plate by a lucite spacer directly above the throat of the diffusion

Figure 19. A, outer chamber wall; B, liquid N_2 shroud; C, constant temperature bath; D, cold diaphragms; E, calibration device; F, signal chopper; G, phase reference; G1, lamp; G2 chopper; G3, photo diode, H, drive magnets; I. BaF_2 window; J, liquid N_2 fill tube; K, nylon knife edge supports; L, bakelite drive shaft; M, synchronous motor; N. Teflon race bearing.

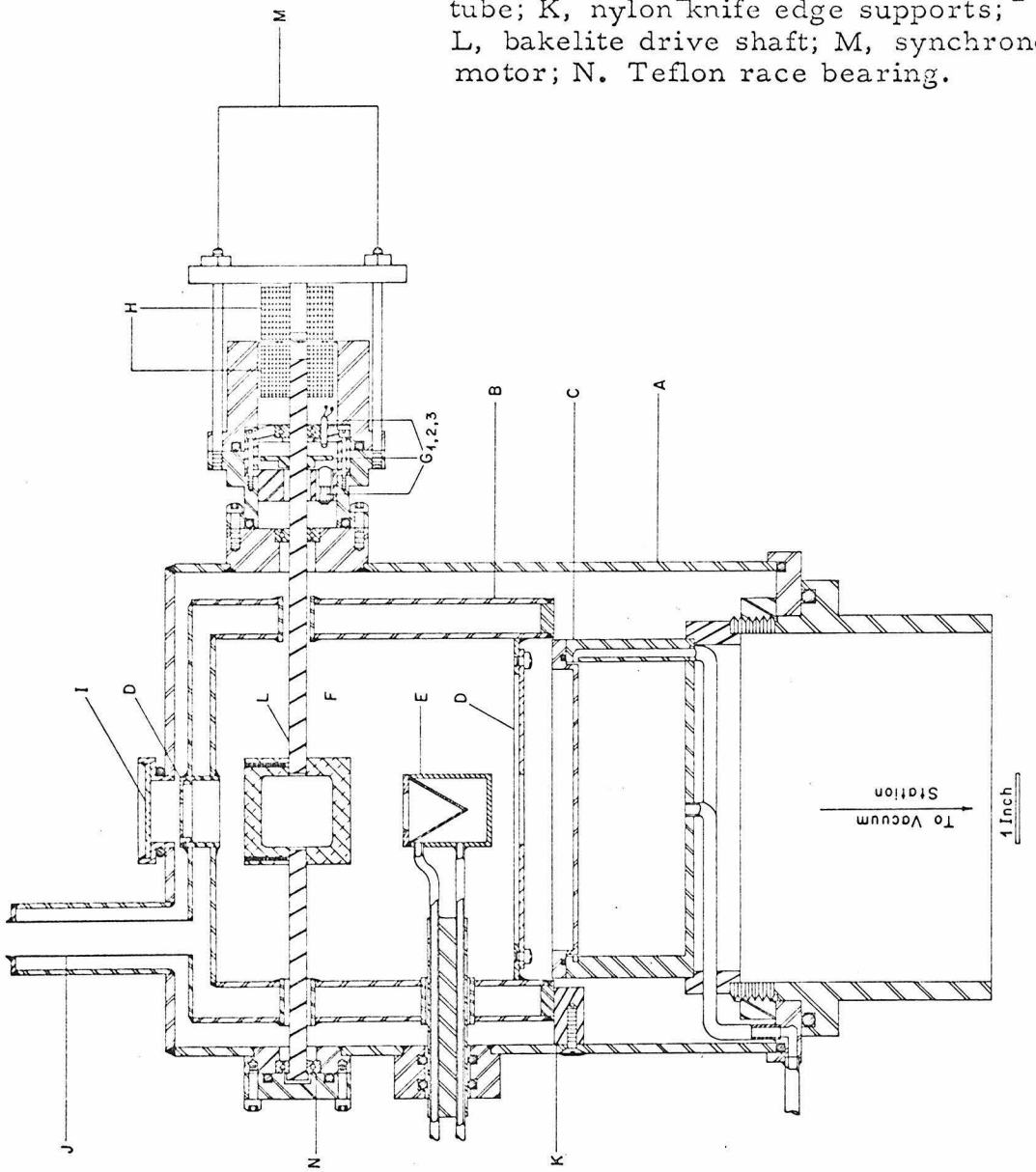

pump. The bath has a removable lid with a quarter-inch depression in its surface which acts as a sample holder. The water inlet is placed at the bottom of the bath while the outlets are at four points along an edge groove concentric with the holder but above its lower surface. This construction does not allow an air bubble to form along the bottom of the holder and therefore provides good thermal contact with the water. Both input and output temperatures of the water flow are monitored. The difference was never more than 1.2° C. The water was not recycled and was heated by an in-line 2500 watt heater. The temperature could be varied continuously from the water main temperature of about 20° to 100° C. The maximum variation over a twenty-four hour period was ± 2° C.

The calibration device is located approximately midway between the sample surface and the chopper. Its function is to provide blackbody, or more accurately, graybody emission at a known temperature. This is accomplished by pumping ice water through the device. The device, shown in Figure 1, consists of a 30° half-angle cone machined into a slightly larger copper cone about one-inch long. This piece is hard soldered into a hollow cylinder containing inlets and outlets for cooling water. The base of the inverted cone is masked with a 1/2" diameter diaphragm slightly larger than the f-16 beam width at that point. The inner surfaces are coated with Krylon Primer. The device can be inserted laterally into the measuring beam, from outside the chamber, obscuring the sample surface,

The chopper is a piece of blackened, round aluminum stock, one and one-half inches in diameter, through which a square opening has been cut in such a way that the circumference of the chopper is equally divided. The chopper is supported by L, bakelite rod shafts, ending in N, Barden Corporation Teflon race ball bearings. The bearings are in the vacuum but remain at the temperature of the outside wall. Attached to one shaft is a second chopper which provides the phase reference signal. The extreme end of the shaft holds a magnet. Directly adjacent is the .020-inch thick stainless steel housing wall of the bearing assembly. Opposite to the interior magnet is mounted M, the exterior 3600 rpm synchronous chopper motor and drive magnet.

The signal chopper is cooled by radiation alone, and a cold diaphragm is placed directly above the chopper to limit any radiation from outside the f16 beam. Another diaphragm, thermally coupled to the nitrogen shroud, is placed between the calibration unit and the sample surface to isolate the two.

In this system a 2mm thick powder sample comes to thermal equilibrium in eight to twelve hours.

Vacuum System

The vacuum system consisted of a pumping station, a base plate through which the bath water lines were led and a nine-inch high, seven-inch diameter, 1/8-inch wall cylindrical stainless steel chamber. The system was evacuated by a four-inch oil diffusion pump (750 liter/sec. at 10^{-3} Torr) with a Freon-cooled baffle backed

by a mechanical pump. The pressure ranged from 10^{-5} to 10^{-6} Torr during experiment runs. The system was usually evacuated in less than an hour. A throttle system was used to avoid evacuating the chamber so rapidly that the powders would be disturbed.

Detection System

The flux emitted from the surface into the cooled cavity passes through the adjacent cold diaphragm and is chopped at 120 Hz. The resulting modulated flux passes out through the second cold f16 diaphragm and is transmitted out of the chamber through the .060" thick BaF_2 vacuum window. The transmission of the window is fairly uniform across the 8-13μ region, falling off rapidly beyond 13μ.

The emerging flux illuminates the slits of a modified Ebert-Fastie grating spectrometer coupled with a liquid hydrogen-cooled, mercury-doped germanium detector. This was the same spectrometer-detector combination used in the telescopic observations. The signal was amplified and synchronously detected using the phase reference signal generated by the phase detector coupled to the chopper shaft. The DC output signal was displayed on a chart recorder and simultaneously digitized and punched on paper tape. The flux received at the detector is the difference between the combined flux from the sample, the diaphragms, the window and the spectrometer on one-half chopper cycle, and the flux from the cold chopper, the diaphragms, the window and the spectrometer on the other half-cycle. The net signal produced is then the difference between the fluxes from the sample and the chopper. Since the chopper is cooled by radiation

to a temperature (approximately 100°K), which is below the minimum detectable temperature of the system, it acts as a zero reference level. The signal which is amplified is that from the sample (or calibration unit) alone. The detector receives energy through a cold 7.6μ long wave pass filter, and the spectrometer grating operates in the first order. The peak signal-to-noise ratio for a sample having a surface temperature at 200°K is about 60:1.

APPENDIX II. SAMPLES AND PREPARATION

The samples shown in Table 1 were used in this study. Each sample was crushed by hand or in a Spex Company "Shatterbox," using a tungsten carbide sample dish. The crushed material was sized using a series of stainless steel Tyler sieves with mesh openings of 589, 295, 147, 74, 43 and 38 microns.

Samples to be measured were loaded into the sample holder, and the holder was tapped with a hammer until the sample was evenly distributed. Precautions were taken to treat all samples uniformly to prevent any wide variations in packing. The thickness of the sample was determined by measuring the length of travel of a binocular microscope tube between the focus on the empty sample holder and the focus on the sample surface.

Sample thicknesses varied from 1 to 3 mm. Thicker samples would have required more time to come to equilibrium, and the surface temperature would have dropped below 180°K, the minimum temperature consistent with good signal-to-noise ratio. Because of the time required for the sample to come to thermal equilibrium and the time required to rewarm the system, only one experimental run could be completed in twenty-four hours.

A total of 304 laboratory spectra were taken, with an average of four spectra made during each experiment run. Emission measurements were repeated on a number of samples to test the reproducibility of the data. Relative emissivities could be reproduced within 5% between measurements of the same sample.

TABLE 1

Sample	Percentage Mineral Phases		Locality
Quartz Monzonite Gneiss	Plagioclase An_{15}	35	Lithonia, Ga.
	Quartz	30	
	Microcline-Microperthite	30	
	Biotite	04.4	
	Muscovite	00.4	
	Others	00.2	
Weathered Quartz Monzonite Gneiss	Kaolinite and other Clays	50	Lithonia, Ga.
	Feldspar	25	
	Quartz	20	
	Vermiculite and Micas	05	
Rhyolite Tuff	Glass	90	Devil's Punch-bowl So. end of Mono Craters Mono, Calif.
	Sanidine	07	
	Quartz	02	
	Oligoclase	01	
San Marcos Gabbro	Plagioclase An_{60}	55	Pala, Calif.
	Hornblende	19	
	Hypersthene	12	
	Augite	10	
	Ores	03	
	Others	01	
Pisgah Basalt	Plagioclase	50	Pisgah Crater San Bernardino Cty., Calif.
	Pyroxene	28	
	Olivine	20	
	Iron Oxide	04	
Websterite	Clinopyroxene	65	Moses Rock Dike, San Juan Cty., Utah
	Orthopyroxene Diopside	35	
Quartz			
Microfine Precipitated Silica, Quso F22	Amorphous SiO_2		Philadelphia Quartz Co.

Table 1 (Continued)

Sample	Percentage Mineral Phases	Locality
Hornblende		
Garnet Almandite		
Olivine		

APPENDIX III. LUNAR POSITION DATA

Table 2 contains a list of all the lunar positions observed. Data for all the points with the exception of Aristarchus, are given in Figures 13-18. Eight spectra were taken of Aristarchus, but in each case the observing conditions were so poor that no useful data were obtained.

The IAU 1961 convention is used for the lunar directions. North is in the direction of Plato, and Mare Crisium, near the first quarter terminator, is in the lunar eastern hemisphere. Using this convention the sun rises in the east on the moon.

The position coordinates are taken from the Orthographic Atlas of the Moon, Edition B (University of Arizona Press, 1960) and are accurate to 0.2°.

TABLE 2 - LUNAR POSITIONS

Position	Aperture size in mm.	Description	Lunar latitude in deg.	Lunar longitude in deg.
Eastern Loop:				
Mare Crisium	1, 1.5, 2	Mare	00 N	60 E
Proclus	1	Bright ray crater	16.2 N	47 E
East of Messier	1	Mare	01.5 S	49 E
Stevinus	1	Bright ray crater	32.3 S	54.1 E
Sina-Cauchy	1	Mare	09 N	35 E
Menelaus	1	Bright ray crater	16.1 N	15.9 E
Sulpicius-Linne	1	Mare	24 N	12 E
South of Callipus	1	Mare border	36 N	11 E
Western Loop:				
Plato	1, 1.5	Partially filled crater	51.5 N	09 W
Mare Vaporum	1	Mare	14 N	04 E
Bruce	1	Small, bright crater in Mare	01.2 N	00.2 E
Ptolemaeus	1	Large old crater	09 S	01 W
Spot in West Alphonsus	1	Black halo crater	13.5 S	04.2 W
Center Alphonsus	1	Central peak	13.3 S	02.8 W
Tycho	1, 1.5	Very bright ray crater	43 S	11.5 W

Table 2 (Cont'd.)

Mare West of Palisa	1	Mare	09.5	S	10.5	W
Copernicus	1, 1.5	Large ray crater	09.8	N	20	W
Miscellaneous						
Kepler	1, 1.5	Bright ray crater	08	N	38	W
Aristarchus	1	Brightest ray crater	23.8	N	46.5	W
Mare Humorum	1, 1.5	Thermally anomalous Mare	22	S	40	W
Center Tranquilitatis	2	Mare with hot spots	08	N	27	E
Center Serenitatis	2	Mare generally free of hot spots	26	N	18	E
Azophi-Sacrabosco	2	Typical Uplands point	22	S	14.5	E

APPENDIX IV. TELESCOPE INSTRUMENTATION

The instruments used for the telescope work were a combination of the photometer described by Westphal et al. (1963), used previously for broad-band infrared photometry, and the grating spectrometer and detector combination used in the present laboratory investigations. This configuration is shown in Figure 20.

The photometer is a two-beam instrument: one beam is focused on the object and the other on the sky next to the object. A three-bladed, aluminized glass chopper, rotating at 10 r.p.s. and mounted at a 45° angle, samples the two beams alternately. The object beam is reflected off the chopper surface and is brought to a focus on the spectrometer entrance slit. This slit consists of an aluminized 45° plate containing several elliptical apertures varying from one-half to 2 mm in effective diameter. The spatial scale at this focus is 20 sec. of arc per mm. Guiding is effected by observing the visible image reflected from the entrance slit plate through an eyepiece.

The sky beam is reflected from a flat placed parallel to and below the chopper blade. The flat is adjustable to allow the signal to be nulled when both beams are on the sky. The beam separation is thirty-five minutes of arc, allowing all points to be covered on the moon without overlap in the sky beam.

The spectrometer is a modified Ebert-Fastie type with a spherical collimator and a 75-line/mm grating blazed for 12μ in the

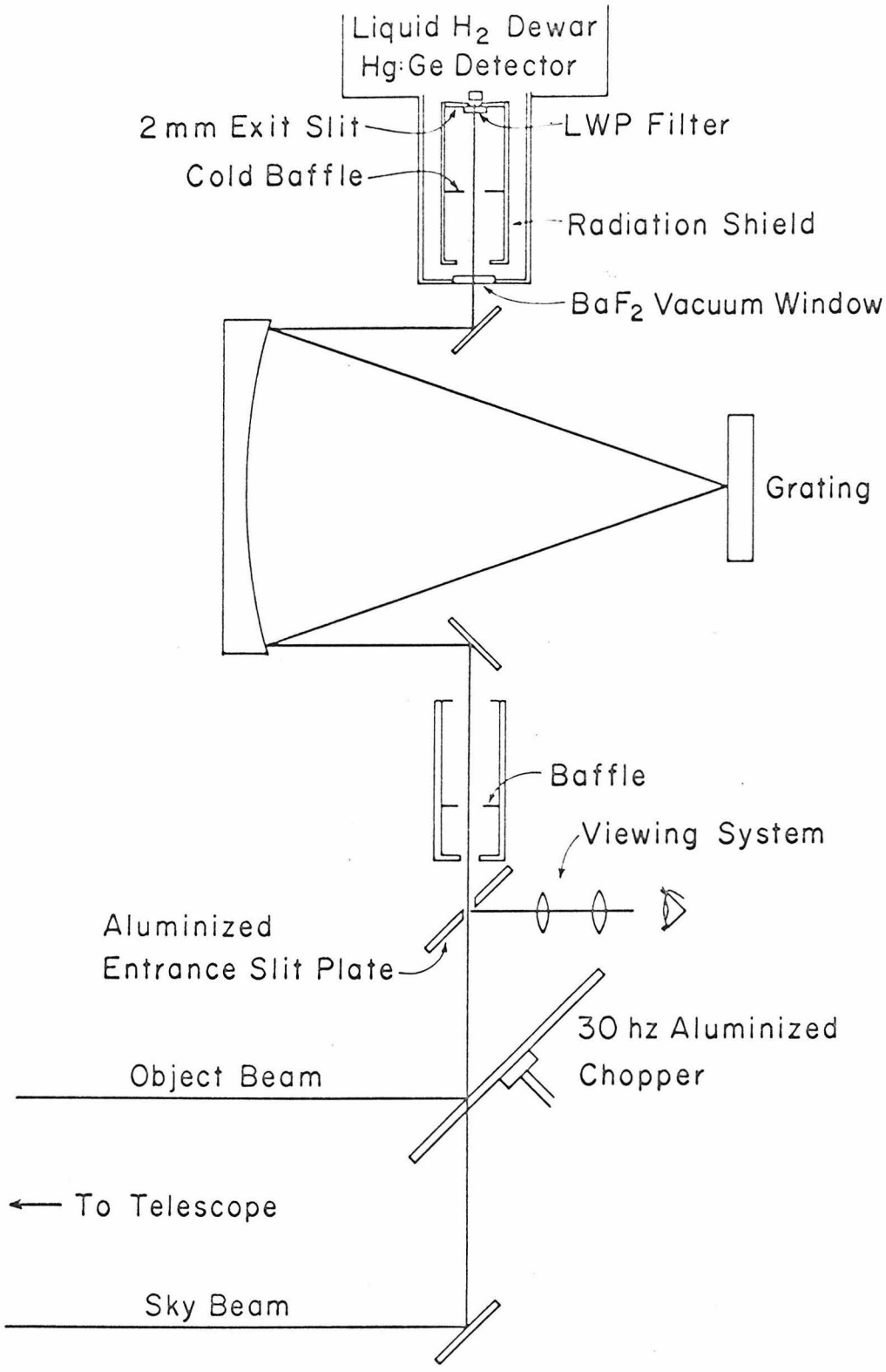

Figure 20. Telescope Instrumentation

first order. Both entrance and exit beams are bent by 45° mirrors to fit the existing photometer and detector packages and to provide for extensive baffling to limit the field of view to f16. This configuration also allows the detector dewar, filled with liquid hydrogen, to remain nearly vertical in normal operation. The detector is mounted on the dewar cold finger at the base of a 12 cm long radiation shield, which is suitably baffled to limit the field of view to f16. A 7.6μ long-wave-pass filter is mounted directly in front of the cell on a plate containing the 2 mm diameter exit slit. Using this configuration, no lenses and only one window are necessary, minimizing transmission losses. The measured wavelength resolution is .08μ at 9μ, or about 110.

The AC signal from the detector was amplified and synchronously rectified. The time constant used was one second. The output signal was recorded on a strip-chart recorder and digitized and punched on paper tape. In a seven-minute spectral scan from 7.5 to 14μ, 950 points were digitized.

APPENDIX V - TELESCOPE DATA PROCESSING

The data processing was handled entirely by an IBM 7094 computer. DC offsets and linear trends were removed from each spectrum. A gaussian digital filter (Westphal, 1965), having a half-width corresponding to one-half of the spectrometer resolution, was applied to the data to remove high frequency components before the quotients were formed. A second order polynomial was fitted by least squares to the quotient points in the regions 8.2 to 9.2 and 10 to 13μ. These wavelength regions were chosen for their high atmospheric transmission to insure that the polynomial fit would not be biased by large excursions in the quotient due to low signal-to-noise ratios.

Data residuals were calculated as a percentage of their departure from the polynomial curve at .01μ intervals from 8.2 to 13μ. A standard deviation for each set of residuals was calculated to provide an unbiased estimate of the quality of the data. Data having a standard deviation greater than 4% were excluded from further analysis. Approximately one-fourth of all the lunar data fell into this category. All the remaining sets of residuals of a given lunar position were weighted inversely proportional to their standard deviations and averaged. The data were then plotted in the format of Figures 13-17.

APPENDIX VI - ATMOSPHERIC TRANSMISSION

Figure 21 is a plot of the relative transmission of the atmosphere between 7.7 and 13.4μ. This curve was obtained by making a spectrum of the sun using the 24-inch telescope diaphragmed to two inches. The spectrum was recorded with the same instrument used in the lunar studies. The data was reduced by using the values for the brightness temperature of the sun at 8.63, 11.10 and 12.02μ given by Saiedy and Goody (1959) and Saiedy (1960).

The 8-13μ window is in reality two windows separated by the deep 9.6μ ozone absorption band. The limits of the window are governed by the broad water-absorption band centered at 6μ and the strong 15μ CO_2 band. Absorbing gases having lines within the window are H_2O, CO_2, N_2O, O_3 and CH_4. At the .08μ resolution, of course, the fine structure of the bands remains unresolved.

The constituent causing the most variability in the atmospheric transmission was water vapor. By far the best observations were made during the local "Santana" conditions, when the relative humidity ranges from 5 to 20%. In spite of poor seeing and gusty winds, the transparency remains constant much of the time.

Figure 22 shows the variability of the atmospheric transmission noise during one night. Both quotients are taken from pairs of spectra made of the same point on the moon on the same night, but three hours apart in time. No clouds were visible and no difference in seeing was observed for the two recordings.

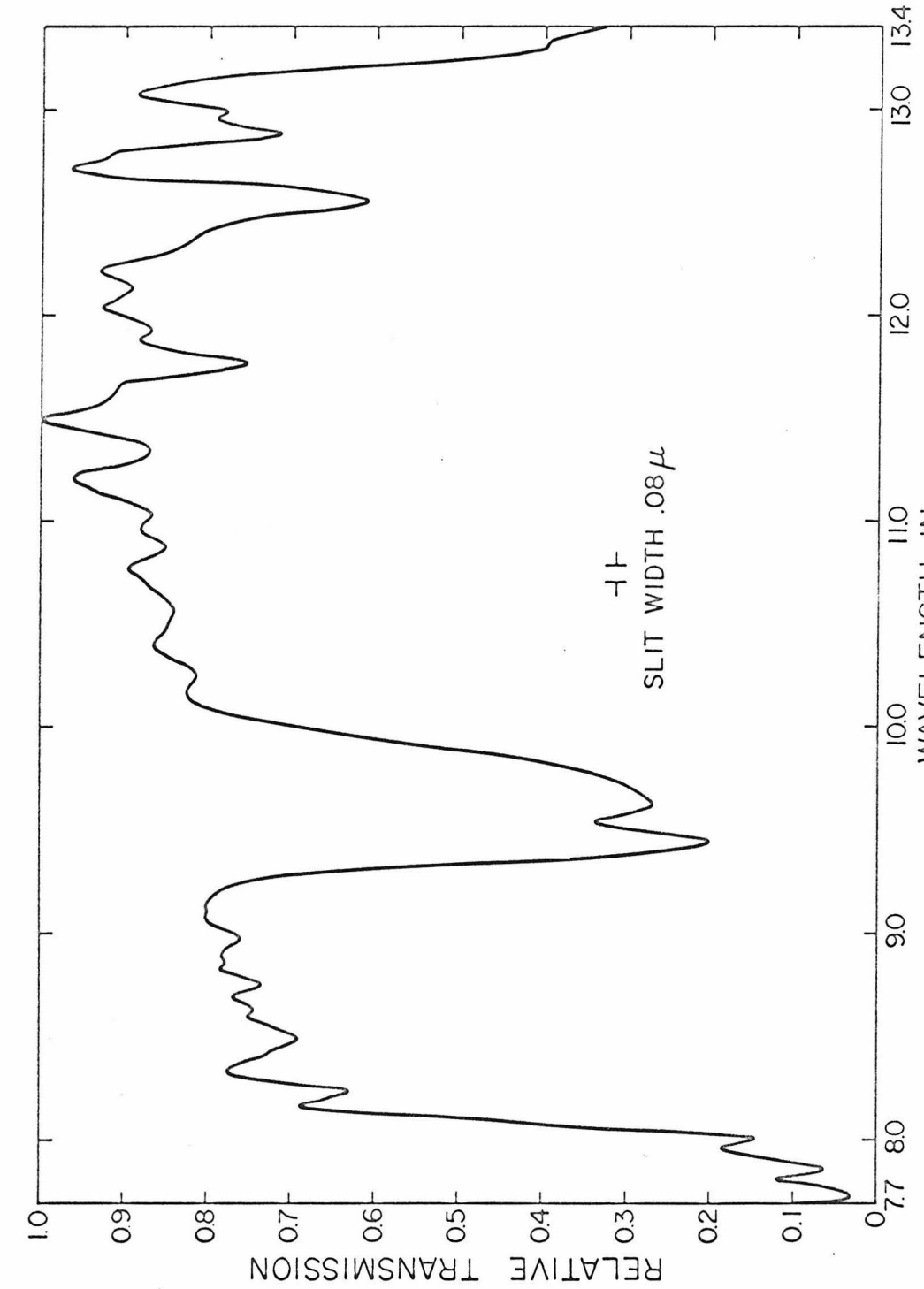

Figure 21. Relative transmission of the atmosphere at sec z = 1.5

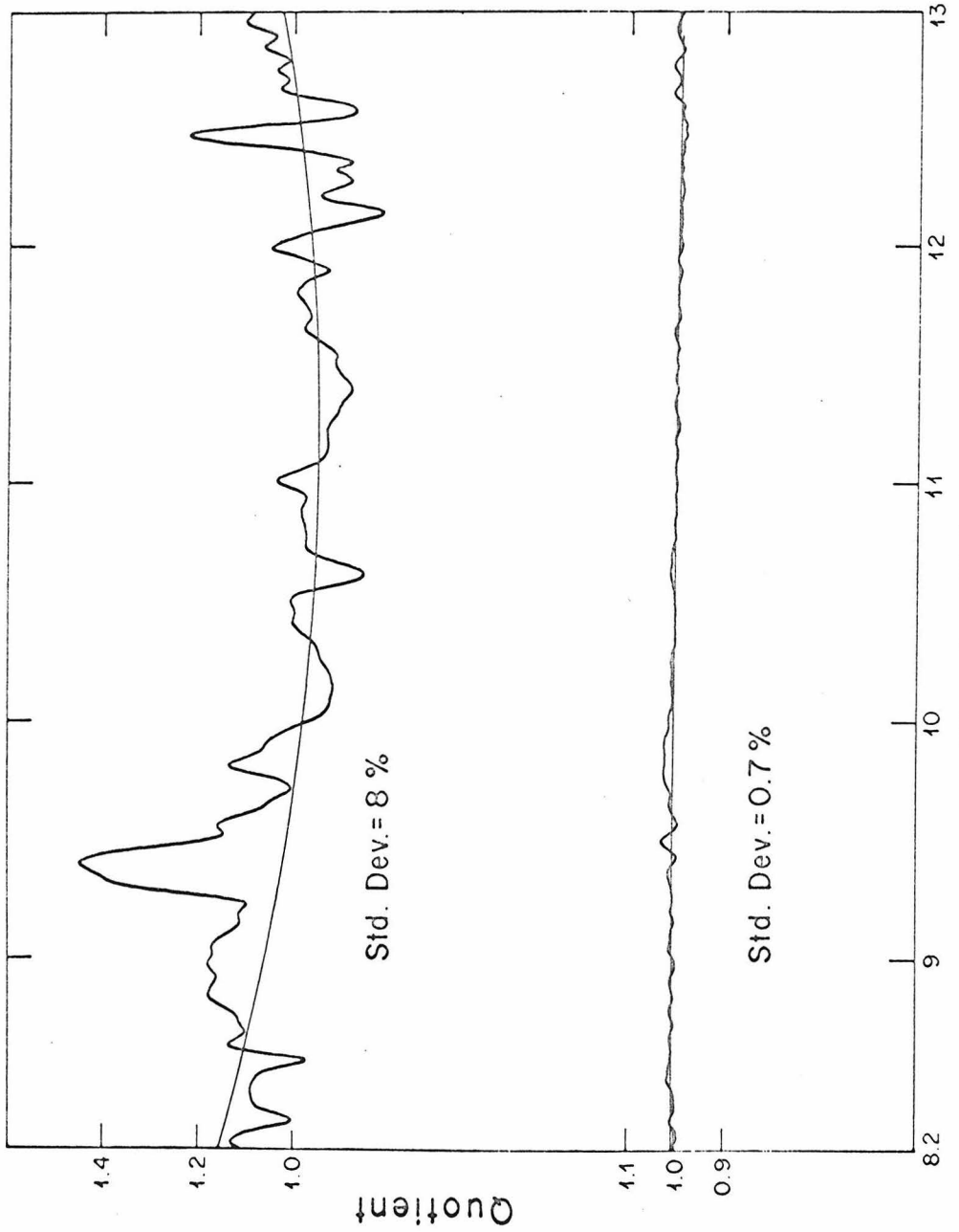

Figure 22. Quotients of pairs of spectra taken of the same point three hours apart in time. Fitted polynomials $P(\lambda)$ are shown.

REFERENCES

Cleek, G. W., The Optical Constants of Some Oxide Glasses in the Strong Absorption Region, Applied Optics 5, 771 (1966).

Conel, J. E., Jet Propulsion Laboratory Technical Memorandum No. 33-243 (1965).

Coyne, G. V., Color Photometry of Selected Features, Astron. J. 69, 538 (1964).

Dollfus, A., "The Polarization of the Moonlight" in Physics and Astronomy of the Moon, Z. Kopal, Ed., Academic Press (1962).

Drake, F., "Radio Measurements of the Moon" in The Nature of the Lunar Surface Layer, W. N. Hess, D. H. Menzel and J. A. O'Keefe, Eds., Johns Hopkins Press, Baltimore (1966).

Gehrels, T., Coffeen, T., and Owings, D., Wavelength Dependence of Polarization, III. The Lunar Surface. Astron. J. 69, 826 (1964).

Goetz, A.F.H. and Bauman, C.A., Apparatus to Measure the Mid-infrared Spectral Emittance of Cold Powders in a Vacuum, Rev. Sci. Inst., in press (1967).

Greer, R. T. and Hapke, B. W., Electron Microprobe Characterization of Microcrystalline Powders Darkened by Simulated Solar Wind Irradiation, J. Geoph. Res., in press (1967).

Hapke, B. W., Effects of a Simulated Solar Wind on the Photometric Properties of Rocks and Powders, N. Y. Acad. Sci., 123, Art. 2, 711-721 (1965).

_____, "Optical Properties of the Moon's Surface" in The Nature of the Lunar Surface Layer, W. N. Hess, D. H. Menzel and J. A. O'Keefe, Eds., Johns Hopkins Press, Baltimore (1966).

Hovis, W. A., Jr., Callahan, W. R., Infrared Reflectance Spectra of Igneous Rocks, Tuffs, and Red Sandstone from 0.5 to 22 Microns, J. Opt. Soc. Am., 56, 639 (1966).

Hunt, G. R. and Salisbury, J. W., Lunar Surface Features; Mid-Infrared Spectral Observations, 146, 641 (1964).

_____, Rapid Remote Sensing by a Spectrum Matching Technique, I. Description and Discussion of the Method, J. Geoph. Res. 71, 2919 (1966).

_____, Salisbury, J. W. and Reed, J. W., Rapid Remote Sensing by Spectrum Matching Technique, II. Application in the Laboratory and in Lunar Observations, Submitted to J. Geoph. Res. (1966).

Hunt, J. M., Wisherd, P. and Bonham, L. C. Infrared Absorption Spectra of Minerals and Other Inorganic Compounds, Anal. Chem. 22, 1478 (1950).

_____, and Turner, D. S., Determination of Mineral Constituents of Rocks by Infrared Spectroscopy, Anal. Chem., 25, 1169 (1959).

Ingrao, H. C., Young, A. T., and Linsky, J. L., A Critical Analysis of Lunar Temperature Measurements in the Infrared, Harvard College Observatory Scientific Report No. 6 (1965).

Jaffe, L. D., et al. Surveyor I, Preliminary Results, Science 152, 1737 (1966).

Launer, P. J., Regularities in the Infrared Absorption Spectra of Silicate Minerals, Am. Mineralogist, 37, 764 (1952).

Lyon, R. J. P., Tuddenham, W. M., and Thompson, C. S., Quantitative Mineralogy in 30 Minutes, Econ. Geol. 54, 1047 (1959).

Lyon, R. J. P., Evaluation of Infrared Spectrophotometry for compositional Analysis of Lunar and Planetary Soils: Part II. Rough and Powdered Surfaces, NASA Contract No. NASr-49(04) (1964).

_____, Analysis of Rocks by Spectral Infrared Emission (8 to 25 microns), Econ. Geol., 60, 715 (1965).

McCracken, C. W. and Dubin, M., Dust Bombardment on the Lunar Surface, NASA Tech. Note D-2100 (1963).

McMahon, H. O., Thermal Radiation from Partially Reflecting Bodies, J. Opt. Soc. of Am., 40, 376 (1950).

Middlehurst, B. M., and Burley, J. M., Chronological Listing of Lunar Events, Goddard Space Flight Center Report No. x-641066-178 (1966).

Miller, F. A., Wilkins, Infrared Spectra and Characteric Frequencies of Inorganic Ions, Anal. Chem., 24, 1253 (1952).

Murcray, F. H., The Spectral Dependence of Lunar Emissivity, J. Geoph. Res., 70, 4959 (1964).

Murray, B. C., Wildey, R. L., Surface Temperature Variations During the Lunar Nighttime, J. Geoph. Res., 63, 4813 (1963).

Petrova, N. N., A Spectrophotometric Study of the Lunar Surface, Sov. Astron. AJ, 1, 128 (1966).

Pettit, E. and Nicholson, S. B., Lunar Radiation and Temperature, Astroph. J. 71, 102-135 (1930).

Pettit, E., Radiation Measurements on the Eclipsed Moon, Astroph. J. 91, 408 (1940).

Saiedy, F., and Goody, R. M., The Solar Emission at 11μ, Royal Astron. Soc. Mon. Notices, 119, 213 (1959).

Saiedy, F. Solar Intensity and Limb Darkening Between 8.6 and 13μ, Royal Astron. Soc. Mon. Notices 121, 483 (1960).

Salisbury, J. W., Samlley, V., and Ronca, L. B., Origin of Linear Elements on Mare Humorum, Nature, 206, 385 (1965).

Shorthill, R. W., Borough, H. C., and Conley, J. M., Enhanced Lunar Thermal Radiation During a Lunar Eclipse, Pub. Astron. Soc. Pac., 72, 481 (1960).

_____, and Saari, J. M., "Recent Discovery of Hot Spots on the Lunar Surface" in The Nature of the Lunar Surface, W. N. Hess, D. H. Menzel and J. A. O'Keefe, Eds, Johns Hopkins Press, Baltimore (1966).

Simon, J. and McMahon, H. O., Study of the Structure of Quartz Cristobalite and Vitreous Solids by Reflection in the Infrared, J. Chem. Phys. 21, 23 (1953).

Sinton, W. M. and Strong, J., Radiometric Observations of Mars, Astrophys. J., 131, 459 (1960).

Su, G. J., Borelli, N. F., and Miller, A. R., An Interpretation of the Infrared Spectra of Silicate Glasses, Physics and Chemistry of Glasses, 3, 167 (1962).

Van Tassel, R. A. and Simon, I., "Thermal Emission Characteristics of Mineral Dusts" in The Lunar Surface Layer, J. Salisbury and P. Glaser, Eds., Academic Press (1964).

Watson, K., Part I: The Thermal Conductivity Measurements of Selected Silicate Powders in Vacuum from 150°-350°K, Doctoral Thesis, California Institute of Technology (1964).

Watson, K. E., and Bauman, C. A., Apparatus to Measure the Thermal Conductivity of Powders in Vacuum from 120 to 350°K, Rev. Sci. Inst. 34, 1235 (1963).

Wehner, G. K., Kenknight, C. and Rosenberg, D. L., Sputtering Rates Under Solar-Wind Bombardment, Planetary Space Sci., 11, 885-895 (1963).

_____, Kenknight, C. E., and Rosenberg, D. L., Modification of the Lunar Surface by Solar Wind Bombardment, Planetary Space Sci., 11, 1257-1261 (1963).

Wesselink, A. J., Heat Conductivity and the Nature of the Lunar Surface, Bull. Astron. Inst. Neth., 10, 351 (1948).

Wesphal, J. A., Murray, B. C., and Martz, D. E., An 8-14 Micron Infrared Astronomical Photometer, App. Opt. 2, 747 (1963).

Westphal, J. A., Some Astronomical Applications of Cross Correlation Techniques, Astroph. J., 142, 1661 (1965).